Sedimentology (2004) **51,** 809–835 doi: 10.1111/j.1365-3091.2004.00652.x

Differentiating the effect of episodic tectonism and eustatic sea-level fluctuations in foreland basins filled by alluvial fans and axial deltaic systems: insights from a three-dimensional stratigraphic forward model

QUINTIJN CLEVIS[1], POPPE L. DE BOER and WOUTER NIJMAN
Sedimentology Group, Faculteit Aardwetenschappen, Utrecht University, Budapestlaan 4, 3500 TA, Utrecht, the Netherlands

ABSTRACT

Many studies of foreland basins have recognized a hierarchical organization in the stacking of sequences deposited by axial-deltaic and alluvial fan systems. The hierarchy is often explained in terms of the competing control of eustasy and pulsed tectonic subsidence and the different frequencies at which these processes operate. Unravelling the relative contributions of tectonic and eustatic controls on the sequence stacking pattern is a fundamental question in foreland basin analysis, yet this is difficult because of the lack of independent stratigraphic evidence. In this study, a three-dimensional numerical model is presented, which aids in the interpretation of alluvial successions in foreland basins filled by transverse and axial depositional systems, under conditions of variable tectonism and eustatic sea-level change. The tectono-sedimentary model is capable of simulating the hierarchical stratigraphic response to both eustatic and tectonic forcing, and is of higher resolution than previous models of foreland basin filling. Numerical results indicate that the onset of tectonic activity is reflected by rapid retrogradation of both depositional systems and by widespread flooding and onlap of carbonate sediments. Syntectonic fluvial patterns on the axial-deltaic plain are dominated by bifurcating channels, swiftly relocating in response to the general rise in relative sea level induced by flexural subsidence. The resulting surface morphology of the axial delta is convex upwards. Syntectonic eustatic sea-level fluctuations result in parasequence-scale packages of retrograding and prograding fan and delta sediments bounded by minor flooding surfaces and type 2 sequence boundaries. Incised channels are rare within the syntectonic parasequences and are formed only during phases of tectonic quiescence when eustatic falls are no longer compensated by the subsidence component in the rise in relative sea level. Suites of amalgamating, axial channels corresponding to multiple eustatic falls delineate the resulting type 1 unconformities. Coarse-grained, incised-channel fills are found in the zone between the alluvial fan fringes and the convex-upward body of the axial delta, as the axial streams tend to migrate towards this zone of maximum accommodation.

Keywords Foreland basin, incised valley fills, relative sea level, stratigraphic simulation.

[1]Present address: Department of Geological Sciences, 2200 Colorado Avenue, Campus Box 399, Boulder, CO 80309-0399, USA (E-mail: qclevis@colorado.edu).

INTRODUCTION

Foreland basins at the transition from under- to oversupply are commonly filled by a combination of two depositional elements: transverse alluvial fans and longitudinal structure-parallel rivers (Kuenen, 1957; Miall, 1981). Modern examples of this association are found on the Po, Indo-Gangetic and Mesopotamian plains (Geddes, 1960; Allen, 1965; Baltzer & Purser, 1990; Ori, 1993; Sinha & Friend, 1994; Gupta, 1997), while ancient examples are well studied in the sedimentary records of the Alpine Molasse Basin (Jin *et al.*, 1995; Schlunegger *et al.*, 1997; Zweigel *et al.*, 1998) and the Pyrenean Foreland Basin (Bentham *et al.*, 1992; Dreyer *et al.*, 1993, 1999; Nijman, 1998). A fundamental problem in interpreting the stratigraphy of these foreland basins is to understand and differentiate between the relative importance of tectonism and eustasy on sequence development and the architectural stacking patterns of both depositional systems (Bhattacharya, 1991; Schwans, 1995; Nijman, 1998; Robinson & Slingerland, 1998; Zweigel *et al.*, 1998; Dreyer *et al.*, 1999).

Alluvial fan and longitudinal river deposits in transitional-type foreland basins typically occur as stacked sequences bounded by unconformities and carbonate-rich mudstone horizons. Each sequence usually reflects continuous deposition at rates of 0·2–0·6 m kyr^{-1} (Mutti *et al.*, 1988; Bentham & Burbank, 1996; Nijman, 1998; Brozovic & Burbank, 2000), while the bounding horizons indicate temporal flooding, low sedimentation rates or erosion. A well-studied example of the internal fluvial architecture of a transitional foreland basin comes from the Eocene Montanyana Group in the Pyrenean Tremp Basin (Marzo *et al.*, 1988; Nijman, 1998; Fig. 1). Here, the stratigraphy is characterized by high-frequency progradation and retrogradation of both transverse alluvial fans and an axial delta, concurrent with a longer term trend of foreland advance of the alluvial fans and axial infilling of the marine accommodation. The sequences are punctuated by onlap of shallow-marine calcareous mudstones, shifts in the location of the axial-channel belt and increases in the degree of amalgamation of channel bodies. These abrupt changes in the architectural stacking pattern represent major sequence boundaries in the Montanyana Group, and are correlatable with basin margin unconformities (Nijman, 1998). The distribution of the Montanyana Group sequence boundaries through time is non-cyclic, and their reoccurrence interval is of the order of 0·2–2·0 Myr. Both the sequence boundaries and the observed shifts in architectural patterns are often explained in terms of pulsating tectonic activity (Puigdefàbregas & Souquet, 1986; Mutti *et al.*, 1988; Nijman, 1998) because of their irregular timing and by analogy with architectural changes predicted by tectonic forcing concepts developed in the late 1980s. Axial and transverse non-marine systems respond differently to the onset of tectonic activity (Blair & Bildeau, 1988; Heller *et al.*, 1988). Thrust-load emplacement causes rapid flexural subsidence in the proximal regions of the basin, with the newly created accommodation occupied first by the finer grained axial-depositional system and subsequently by alluvial fans. The response of the alluvial fans in terms of gravel front progradation is thought to lag behind the onset of tectonic activity because these systems depend on the relatively slow denudation of the newly created topography for their sediment supply (Schumm, 1963), or because of temporal storage and rerouting of sediment behind linear thrust structures, as seen in megafans in overfilled foreland basins (Hirst & Nichols, 1986, Gupta, 1997). In addition, their progradation is inhibited by the high rates of syntectonic subsidence close to the fault front. In most cases, the rate of proximal accommodation creation exceeds the rate of sediment supply from the rejuvenated hinterland, and the alluvial fans initially retreat towards the thrust front (Heller *et al.*, 1988; Schlager, 1993). The externally sourced axial depositional system can take advantage of the sluggish response of the alluvial fans by occupying the newly created depression swiftly because of their low depositional slope and continuous high supply of sediment. When the basin fill is close to sea level, the onset of subsidence results in a punctuated, basin-wide flooding, marked by the deposition of coals, marls or carbonates, depending on the basin configuration and latitude. Later, during ongoing tectonic activity, the balance between the rate of subsidence and the rate of alluvial fan progradation controls the position of the axial system as the axial streams tend to occupy the depressions between fan fringes and the previously deposited axial delta.

The stratigraphic architecture in the Pyrenean example (Fig. 1) is explained (Nijman, 1998) in terms of episodic tectonism, with transient fan progradation and retrogradation interpreted as phases of moderate orogenic uplift linked to flexural generation of accommodation. Shifts

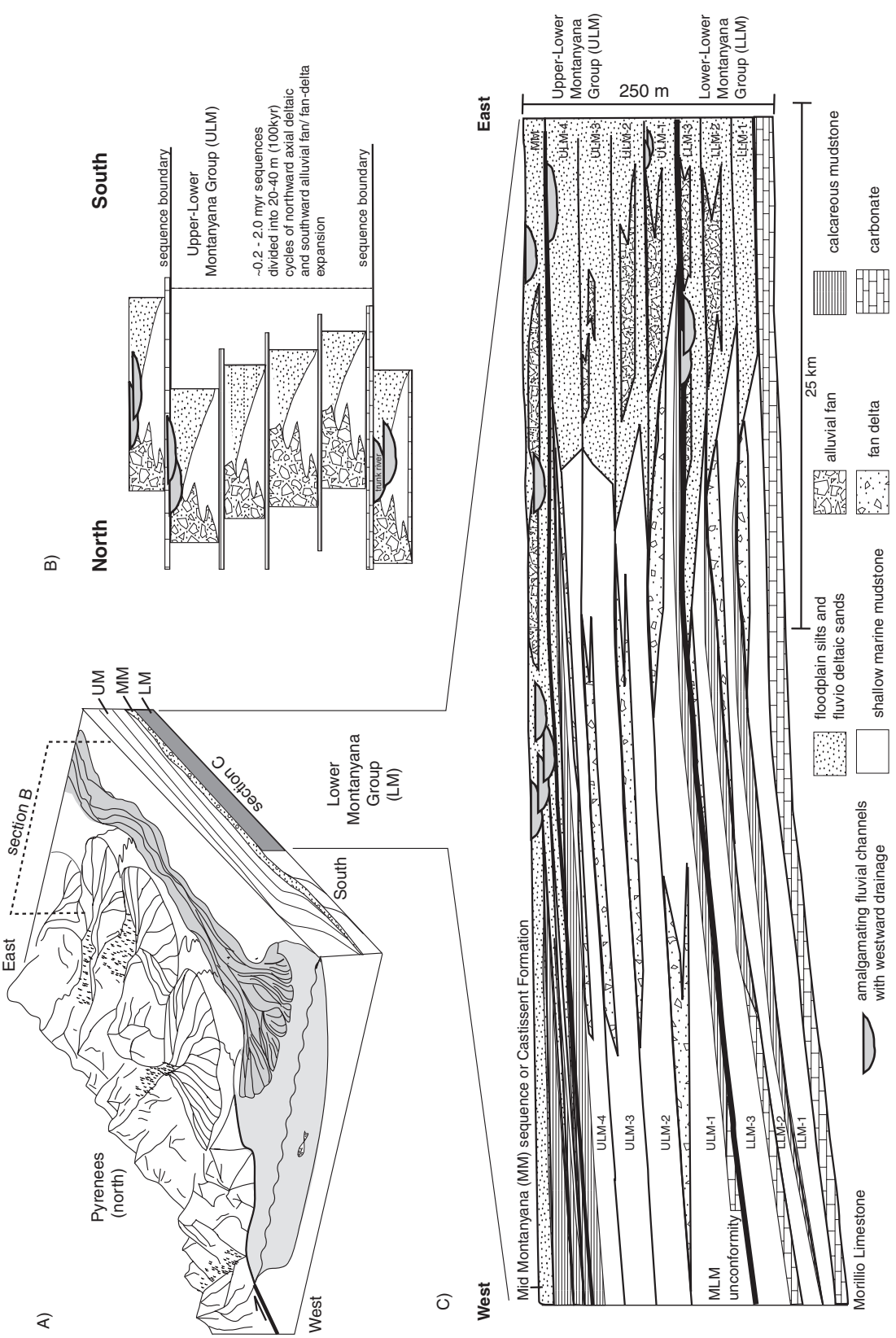

Fig. 1. Eocene drainage configuration of the Tremp Basin in the Spanish Pyrenees, showing transverse alluvial fans and an axial river draining into a marine embayment (A). The north–south section B shows schematically the cycle architecture in the Upper Lower Montanyana (ULM) sequence of prograding alluvial fans and axial-deltaic sediments bounded by minor flooding surfaces and prominent sequence boundaries (based on Nijman, 1998; Fig. 16). Longitudinal section C shows the complete Lower Montanyana Group (53–51·7 Myr), with major sequences Lower Lower Montanyana (LLM) and Upper Lower Montanyana (ULM), divided into smaller cycles (simplified after Tremp Basin section D in Nijman & van Oosterhout, 1994).

and amalgamation of the axial fluvial system, and the concurrent flooding events, are interpreted as short accelerations (0·2–2·0 Myr) in tectonic activity and subsidence, capable of reorganizing the drainage patterns in the basin (Nijman, 1998).

The stratigraphic response to tectonic processes in the Pyrenean and other foreland basins is often complicated by a higher order stratal pattern with a frequency close to 100 kyr (Fig. 1). These are patterns of repetitive growth of the fans (Nijman, 1998) or upward-coarsening and upward-shallowing progradational axial delta packages, bounded by minor flooding surfaces (i.e. parasequences). The fan cycles and parasequences could reflect short-term variations in thrust propagation (Houston *et al.*, 2000) or climate-induced fluctuations in sediment supply (De Boer *et al.*, 1991; Weltje *et al.*, 1996), but are often explained by eustatic sea-level change (Bhattacharya, 1991; Dreyer *et al.*, 1999; Chen *et al.*, 2001; Plint *et al.*, 2001). Interpreting foreland basin stratigraphy is therefore difficult because the relative importance of tectonism and eustasy in determining sequence development and architectural stacking patterns is not always apparent.

In this paper, a three-dimensional stratigraphic forward model is constructed to facilitate the interpretation of ancient alluvial successions generated by a combination of tectonism and eustasy. The aim is to investigate whether diagnostic stratigraphic patterns can be generated by combinations of these two basic controls and to compare the model results with the current interpretations of the Tremp Basin (Clevis, 2003). The quantitative model simulates the interaction between sea-level change, variable thrust activity, flexure, orogenic denudation and sediment transport on alluvial fans, in axial channels and in the shallow-marine realm. Animations of the landscape evolution and recorded time series of denudation and deposition rates are used to investigate geomorphic processes and the associated stratigraphic response. The resulting foreland basin stratigraphy is visualized by means of cross-sections, fence diagrams and sediment voxel bodies, which show the lithology and evolving depositional architecture.

MODELLING METHOD

Comparison with earlier modelling studies

During the previous decade, process-based models of long-term sedimentation have become widely used tools in theoretical and applied basin studies. A thorough overview of the developments in the field is provided by Paola (2000). The early generation of two-dimensional foreland basin models increased the understanding of sedimentation responses to tectonic loading and unloading (Flemings & Jordan, 1990; Sinclair *et al.*, 1991; Peper & de Boer, 1995). Subsequent three-dimensional models echoed their conclusions and added along-strike variation in tectonic convergence rate, subsidence, drainage patterns and stratigraphy (Johnson & Beaumont, 1995; Garcia-Castellanos *et al.*, 1997; Garcia-Castellanos, 2002). Despite the numerical complexity involved in these models, the spatial and vertical resolution of the synthetic stratigraphic sections generated is often poor, and they do not discriminate depositional facies or incorporate grain-size variations. Consequently, the model results are only suitable for illustrating large-scale, geodynamic concepts, and are difficult to compare directly with sedimentological field studies that gather data at higher resolution. Models that operate at an outcrop scale have been developed in the recent past (Ritchie *et al.*, 1999; Hardy & Gawthorpe, 2002; Gawthorpe *et al.*, 2003), and they give important insights into the response of fan delta systems to differential fault-slip rates and eustatic sea-level change in small half-graben basins. However, important elements controlling foreland basin stratigraphy, such as thrusting, flexural isostasy, hinterland drainage basin development, deltaic bifurcation of water and sediment flow, and sediment sorting, are not included in these models.

In this study, a model is developed to bridge the gap between large-scale geodynamic and smaller scale outcrop models. The modelled time span and spatial dimensions of the set-up are smaller than those of the larger foreland basin models because of computational limitations. The model operates on a 150×150 rectangular grid with a spatial resolution of 500 m (Fig. 2). This spatial resolution is a compromise between acceptable run times, the ability to incorporate the geodynamic process over time spans of 2·0–3·0 Myr over an area the size of a small foreland basin and to have realism in the stratigraphic output. Discretization of 500 m is of higher resolution than that applied in other three-dimensional foreland basin models (15 km, Johnson & Beaumont, 1995; 1 km, Tucker & Slingerland, 1996; 5 km, Garcia-Castellanos, 2002). Ideally, the spatial resolution should be close to the channel width (e.g. 40 m, Gawthorpe *et al.*, 2003), but this demands an

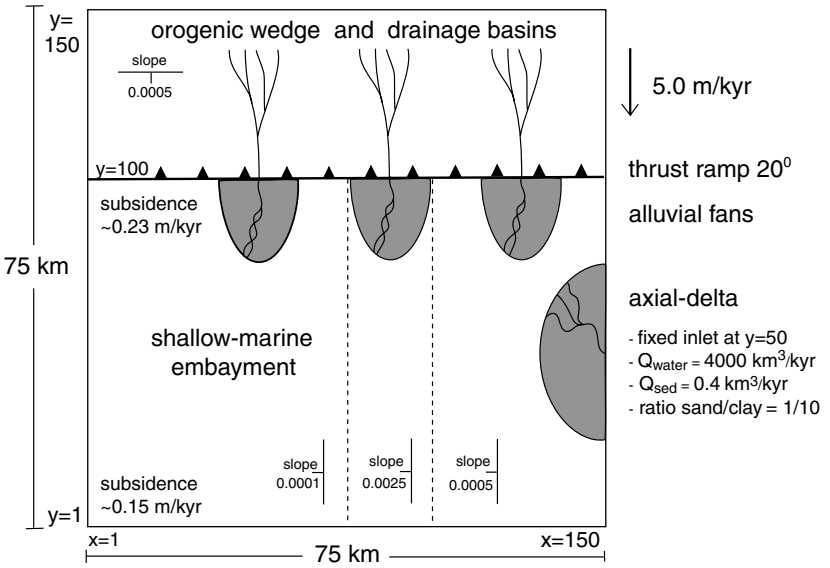

Fig. 2. Plan view of the model set-up, comprising a proximal foreland basin separated from the orogenic wedge by a hinterland-dipping thrust fault. The initial surface slopes and the fixed inlet position of the axial system are indicated. The rate of syntectonic subsidence diminishes basinward due to the shape of the flexural response to loading of the orogenic wedge. Drainage basin morphologies and alluvial fans evolve automatically. The model area is 75 × 75 km and uses a 150 × 150 rectangular matrix of 500 m square cells.

increase in computer power. The 'channel' cells visualized in the present model should thus not be interpreted as true channels but, instead, as channel belts as these are objects of comparable size (Mackey & Bridge, 1995).

Model starting conditions are a nearly flat orogen-foreland basin landscape, where the relative proportions of orogen vs. basin are tailored to the palaeogeography of the Tremp Basin (Figs 1 and 2). The small slopes in the set-up are spiked with a 1% random perturbation in order to initiate drainage patterns. No uplifted source terrain is present as a model run starts, and shallow-marine conditions prevail everywhere on the computational grid. The marine basin persists in the foreland due to thrusting and flexural subsidence but is progressively filled by the advance of alluvial fans and an axial alluvial system. The rate of thrust advance and orogenic uplift is given by an on/off curve where the duration of tectonic pulses is comparable to the minimal durations of the sequences in the Tremp Basin. This simplified form of orogenic uplift is calculated in steps of 2 kyr, and the corresponding flexural response is applied incrementally to the model space every geomorphic process time step of 10 years (Clevis *et al.*, 2003). The drainage basin morphology and the positions of the alluvial-fan sources are established automatically during the first 200 kyr in a model run. Basic geomorphic properties such as fan spacing are a function of uplift rates, bedrock erodibility and the initial surface perturbation. The effect of a range of erodibility and uplift values on the morphologies and long-term sediment yields was investigated by Clevis *et al.* (2003).

Orogenic denudation and excavation of the drainage basins during the geomorphic time steps is performed by bedrock collapse, bedrock incision and bedrock-to-regolith conversion, i.e. weathering (Fig. 3). The released sediment is distributed over alluvial fans following steepest descent and bifurcating routing schemes while using stream power-type equations for stream transport capacity (Clevis *et al.*, 2003). An important additional sediment source enters the model basin in the form of an axial fluvio-deltaic system (Fig. 2). The inlet position and sediment influx are kept constant throughout the experiment, because it is still debated whether the axial system in the Tremp Basin was sourced by upstream alluvial fans in the north-east (Marzo *et al.*, 1988) or by remote drainage basins on a southern forebulge high (Nijman, 1998). The constant water and sediment supply rates to this system, 4000 $km^3\ kyr^{-1}$ and 0·4 $km^3\ kyr^{-1}$, are based on the time-averaged volumetric sedimentation rates of the Lower Montanyana Group in the Tremp Basin (Fig. 1). The supply ratio is derived from the general notion that the average sediment–water discharge ratio for large rivers fluctuates around 1:10 000 (Milliman & Syvitski, 1992). The axial sediment entering the system is composed of 10% sand and 90% finer grained sediment (Burgess & Hovius, 1998). Both alluvial fan and axial sediments are routed towards the shallow-marine embayment where they are

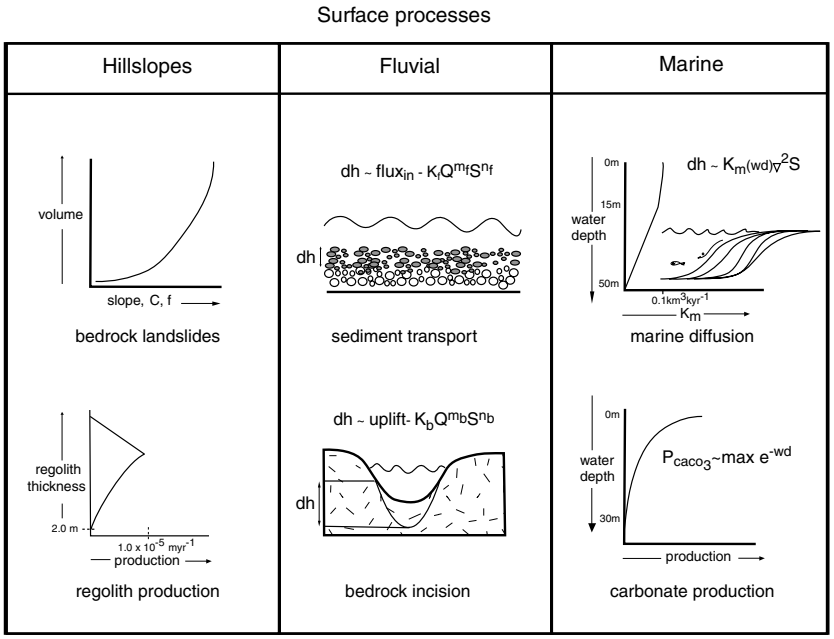

Fig. 3. Diagram summarizing the main surface processes used to generate and transport sediment in the drainage basins and depositional sections of the modelled foreland setting. Selected literature sources for the methods used are: bedrock landslides (Spangler & Handy, 1982; Densmore *et al.*, 1998), regolith production (Heimsath *et al.*, 1997), sediment transport (Howard *et al.*, 1994; Tucker & Slingerland, 1996), bedrock incision (idem.), marine diffusion (Kenyon & Turcotte, 1985) and carbonate production (Boscher & Schlager, 1992).

deposited in a delta or leave the model grid along the axial gradient. Marine cells, deprived of clastic input, simulate carbonate production *in situ*.

Surface processes

Stream power law sediment transport

Sediment transport both on the alluvial fans and in the axial channels is evaluated with a stream power-type equation, which states that the capacity to carry sediment is proportional to the product of local slope S and water discharge Q in the channel (Howard, 1994; Tucker & Slingerland, 1996). In the absence of tectonic subsidence or uplift, the change in height of a channel belt cell is a function of the changes in carrying capacity along the transport path:

$$\frac{\partial h_{all}}{\partial t} = -\frac{K_f}{W}\left(\frac{\partial Q^{m_f} S^{n_f}}{\partial x} + \frac{\partial Q^{m_f} S^{n_f}}{\partial y}\right) \qquad (1)$$

where W is the channel width, which can be approximated as the square root of local discharge Q using an empirical equation (Leopold & Maddock, 1953), and K_f is the fluvial transport coefficient. Eq. (1) is derived from engineering time-scale formulae for bedload transport, and the value of K_f can be approximated by substitution giving a value ranging between 0·001 and 1·0, depending on the assumptions taken during the derivation (Tucker & Slingerland, 1996; Murray & Paola, 1997). In this study, two intermediate values for K_f are applied, one for the alluvial fans (0·01) and one for the axial fluvio-deltaic system (0·1). These values give numerically stable equilibrium slopes for alluvial fans and the axial delta, and realistic long-term sedimentation rates in combination with the spatial discretization and the geomorphic time step chosen. A similar 10-fold difference in transport coefficient between the coarse fan and finer axial sediments has also been applied successfully in a study of extensional basins (Marr *et al.*, 2000) to model the difference in transportability between both fractions. As in diffusion-based stratigraphic modelling studies, there is a wide range in possible values of the transport coefficient K_f in the stream power-type formulation, depending on the spatial and temporal discretization used (Anderson & Humprey, 1990; Paola, 2000; Quiquerez *et al.*, 2000). The theoretical background of the stream power equation is well discussed by Whipple & Tucker (1999, 2002) and Tucker & Whipple (2002), focusing on the value of the transport exponents m_f and n_f, which can be as high as $m_f = n_f = 2{\cdot}0$, if Enstein–Brown is used in the derivation of the stream power equation (Willgoose *et al.*, 1991). In this study, a slope exponent of $n_f = 1{\cdot}0$ is used, ensuring numerically stable transport while distributing sediment over multiple downstream cell directions, and $m_f = 1{\cdot}5$, because it enhances channellization and incision of flow at stream confluences (e.g. Murray & Paola, 1997; Crave & Davy, 2001). Each fluvial system carries a sediment load composed

of two grain-size fractions. During the multiple evaluations of erosion and deposition along the stream paths through the computational grid, the coarse fractions are segregated from the finer ones using the perfect sorting principle, which is based on selective deposition of the least transportable fractions (Paola *et al.*, 1992; Clevis *et al.*, 2003).

Bedrock incision

In the absence of a sediment cover, the change in height of a cell is determined by the rate of bedrock incision, which is again a function of discharge and slope (Howard, 1994):

$$\frac{\partial h_b}{\partial t} = -K_b Q^{m_b} S^{n_b} \tag{2}$$

where K_b is the bedrock erodibility coefficient with a value of $1{\cdot}0 \times 10^{-4}$ yr$^{-2/3}$. This erodibility value lies in the middle of the range derived by both inverse modelling of fluvial bedrock profiles (Stock & Montgomery, 1999) and time-averaged denudation rates found in fission-track field studies (Morris & Sinclair, 1997; Meigs *et al.*, 1999; Kirky *et al.*, 2002). The effect of a wider range of values on drainage basin morphology and sediment yield is explored by Clevis *et al.* (2003) and is not discussed further here. Exponents m_b and n_b are 1/3 and 2/3, respectively, as these values result in a well-calibrated fit between the modelled and observed topography of the Zagros fold-and-thrust belt (Tucker, 1996). Sediment produced by bedrock incision is composed of 50% gravel and 50% sand and is distributed further downstream by fluvial transport (Eq. 1).

Bedrock collapse

In actively deforming regions, bedrock landsliding is an important contributor to denudation (Hovius *et al.*, 1997). However, landslides are complex sporadic events for which it is hard to derive a time-averaged denudation rate. It depends on the interaction between hillslope gradient, rock strength, internal friction and the occurrence of seismic events (Schmidt & Montgomery, 1995; Densmore *et al.*, 1998). The local potential failure is assessed using the Culmann slope stability criterion (Fig. 4; Spangler & Handy, 1982; Densmore *et al.*, 1998). This criterion states that the maximum stable hillside slope will be reached when the effective weight (F_{eff}) on the potential failure plane is balanced by the shear resistance on this plane (F_{r}):

$$F_{eff} = F_w \sin\theta \tag{3}$$

$$F_r = CL + F_w \cos\theta \tan\phi \tag{4}$$

where F_{w} is the weight of the material, θ the slope of the failure plane, L the length of the failure plane, C the cohesion and ϕ the friction angle on the plane (Spangler & Handy, 1982; Densmore *et al.*, 1998). Failure will occur at the critical fault plane if $F_{eff} = F_r$. In this situation, the cohesion on the failure plane is expressed as:

$$C = \frac{1}{2}\rho g H \frac{\sin(\beta - \theta_c)\sin(\theta_c - \phi)}{\sin(\beta)\cos(\phi)} \tag{5}$$

where ρ is the density of the rock, g the gravitation constant, H is the elevation difference between a stable cell and the collapsing cell and β the surface slope of the landslide envelope (Fig. 4). The derivative of the cohesion with respect to the failure plane slope is:

$$\frac{\partial C}{\partial \theta} = \frac{1}{2}\rho g H \frac{\sin(\beta - 2\theta_c + \phi)}{\sin(\beta)\cos(\phi)} \tag{6}$$

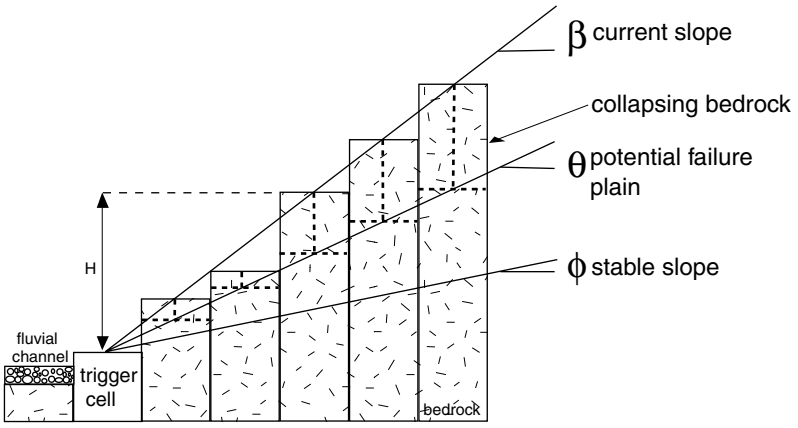

Fig. 4. Two-dimensional diagram of the geometry involved in the evaluation of a bedrock landslide envelope. If collapse takes place, the failure plane becomes the new surface slope, and the material is routed via the target cell towards a nearby fluvial cell as sediment. See text for discussion.

so that C is maximized at $\theta_C = 1/2(\beta + \phi)$. The stable maximum height of the hillslope is found by substituting θ_C into Eq. (6):

$$H_c = \frac{4C}{\rho g} \frac{\sin\beta \cos\phi}{[1 - \cos(\beta - \phi)]} \quad (7)$$

The probability of failure and the resulting landslide can now be expressed as the ratio of the actual hillslope height vs. the maximum critical height according to Eq. (7):

$$P_{collapse} = H/H_c \quad (8)$$

The landslide probability ranges between 0 and 1 and is evaluated using a random number routine. A positive test for a single hillslope cell results in application of the criterion on surrounding potential unstable hillslope cells. The size of the landslide is determined by accumulating all failed mass around the trigger cell of the landslide. The receiving cell of the landslide is the cell holding the steepest slope with the triggering cell (Fig. 4). The landslide is distributed further downstream as a sediment mass flow. The shape of the mass-flow deposit is determined by an empirical determined run-out length ($\approx$ 5 km; Blair, 1999) and the possibility of spreading in multiple directions. During mass-flow routing over the grid, the debris fills in irregular topography and subsequently increases the amount of sediment on valley floors and alluvial fan apices. Mass-flow sediments are subsequently reworked by fluvial erosion and deposition (Eq. 1).

Bedrock to regolith conversion

Regolith is produced by *in situ* chemical weathering of bedrock. Recent studies based on the decay of cosmogenic nuclides indicate that regolith production rates are around $1{\cdot}0 \times 10^{-5}$ –$5{\cdot}0 \times 10^{-5}$ m yr^{-1} for semi-arid areas (western United States, Bierman, 1994) and $5{\cdot}0 \times 10^{-6}$ m yr^{-1} for Alpine areas (Small *et al.*, 1999). These studies have confirmed that weathering rates are faster beneath a certain regolith cover (Heimsath *et al.*, 1997), but decay with increasing cover thickness. According to Densmore *et al.* (1998), the regolith production curve in the model starts with a bare bedrock production rate, increasing linearly to a maximum rate at the regolith thickness optimum, followed by an exponential decrease with increasing regolith thickness (Fig. 3). Regolith is produced in model cells that do not act as drainage outlets for upstream cells. The composition of the regolith produced is 10% coarse and 90% fine-grained sand.

Marine deposition

In the model, a fluvial channel entering the marine realm is instructed to deposit all its bedload until the local accommodation below base level is filled. Excess sediment is distributed to neighbouring marine cells in proportion to the gradient. Within the marine realm, sediment transport is modelled by diffusion because of its ability to produce realistic looking clinoform profiles in deltaic fronts (Kenyon & Turcotte, 1985; Syvitski & Daughney, 1992). Making the diffusivity coefficient K_m water depth dependent enhances this property, simulating the decrease in erosive energy in the coastal area with increasing water depth. The values of K_m are maximum above wave base depth ($0{\cdot}1$ km^3 kyr^{-1} at 15 m) and decrease linearly below this depth (Fig. 3). The marine sediment flux is a function of the water depth-dependent diffusion coefficient K_m and the local slope in three dimensions, ∇S:

$$Q_{sed} = K_m(wd)\nabla S \quad (9)$$

Combined with the continuity equation, this transport equation gives the rate of elevation change for a marine cell:

$$\left.\frac{dh}{dt}\right|_{marine} = -K_m(wd)\nabla^2 S \quad (10)$$

Carbonate deposition

Carbonate-producing organisms are dependent on the intensity of light penetrating through the water column for their growth and are hindered by the presence of clastic sediment. Therefore, a depth-dependent carbonate production law (Demicco, 1998) is applied to the marine model cells (Fig. 3), but only to those that do not receive any clastic input during the specific time step. The carbonate production rate P decreases exponentially with increasing water depth wd

$$P_{carb} = max_{carb} e^{-wd} \quad (11)$$

There is a high variability in the maximum carbonate production rate (max_{carb}) proposed by various authors (for an overview, see Boscher & Schlager, 1992). In this study, the relatively low average sedimentation rates obtained from the Morillio and Guarra limestones ($0{\cdot}1$ m kyr^{-1}, Eocene Pyrenean foreland) are adopted as these limestones formed in a basin with a high rate of clastic supply (Bentham *et al.*, 1992; Molenaar & Martinius, 1996; Nijman, 1998).

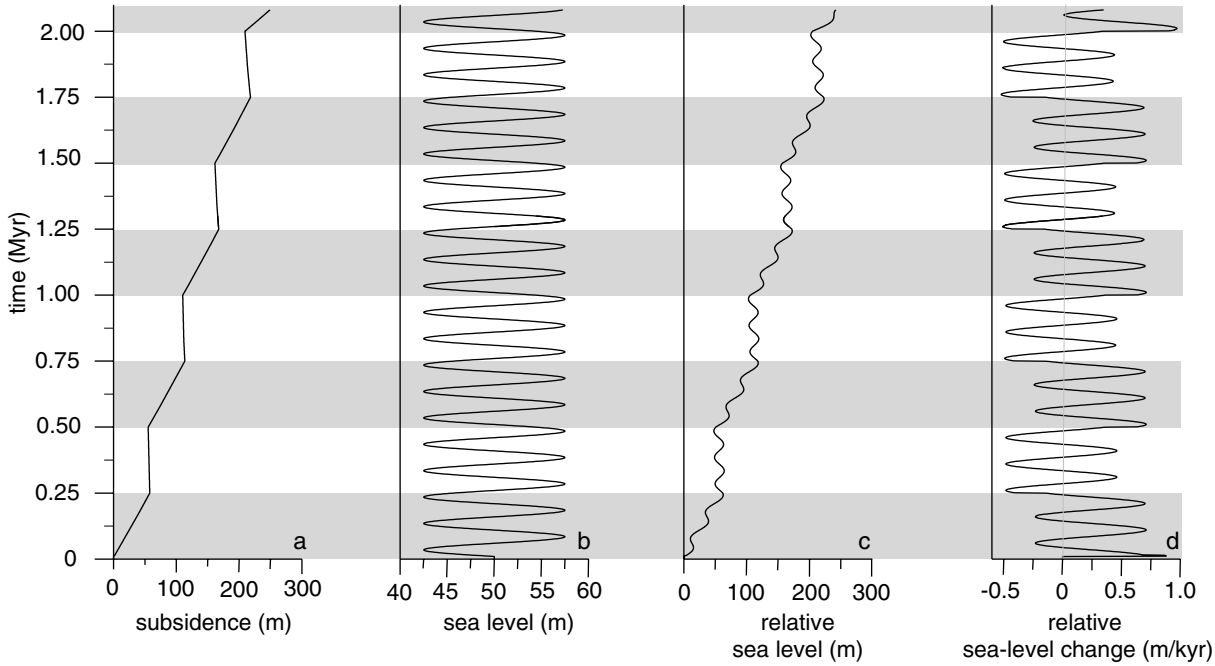

Fig. 5. Curves of the external forcing applied to the model space as a function of simulation time (over 2·0 Myr). The stepped flexural subsidence curve is the effect of pulsed thrust-load emplacement with a periodicity of 250 kyr (a). The superposed eustatic sea-level fluctuation had a periodicity of 100 kyr and amplitude of 7·5 m (b). The resulting composite curve of relative sea-level is depicted in (c) but also its derivative, the rate of relative sea-level change (d). Grey bands represent phases of tectonic activity. See Figs 9–11 for the corresponding stratigraphy.

Tectonic processes

Thrusting of the orogenic block over the developing foreland is modelled using a velocity description of deformation (Hardy & Poblet, 1995). A detailed explanation of the method is given by Clevis *et al.* (2003). The thrust-fault tip and the wedge of hangingwall bedrock migrate basinward with a rate of 5 m kyr^{-1} during phases of tectonic activity, and they are able to cover sediments that were previously deposited at the fault front as the structure advances on to the foreland. This is facilitated in the model by adapting a linked-list data structure for the stratigraphy (Oualine, 1997). All sediment layers and bedrock layers are stored as vertical linked lists of layer data packages containing grain size, age, provenance, etc. and pointers to the surrounding layers. The lists are attached to specific cell locations in the model domain. The upper parts of the stratigraphic layer lists in the foreland are continuously updated by erosion and deposition processes, but can also be modified by tectonic advection of a bedrock wedge into or on to the lists. This depends on the local configuration at the fault front. When the alluvial fan apices cover the tectonic front, the fault tip is extended according to the velocity field, and the bedrock is advected into the list, while conserving the original angle of the thrust fault. If the fan apices are lower than the fault tip, bedrock will be advected on to the lists, and the thrust fault will adapt to the local topography by flattening its angle. This is the most common case and results in ramping and burying of syntectonic sediments while the drainage basin outlets feeding the alluvial fans are uplifted and translated towards the foreland.

A two-dimensional analytical Green Function solution for broken-plate flexure is incorporated in the model (Slingerland *et al.*, 1993) to limit computational effort. The state of bending due to thrust and sediment loading is calculated in three orogen-perpendicular sections at grid locations $x = 25$, 75 and 125, every 2 kyr (Fig. 2), using an effective elastic thickness (EET) of 15 km. Next, the predicted deflection is distributed over the grid by linear interpolation and applied to the entire model space incrementally during the smaller surface process time steps of 10 yr. The boundaries for the broken-plate solution are positioned at $y = 150$ and $y = -300$. So, in contrast to the surface processes, the flexure is calculated on an area comparable to a complete foreland basin. Flexure is a three-dimensional problem and should be calculated as such (Wees

& Cloetingh, 1994; Hodgetts *et al.*, 1998). However, the main load is the moving linear thrust wedge, and a full three-dimensional solution would result in a similar linear depression to that generated by the current method.

Tectonic and eustatic forcing

During the scenario modelled, the foreland basin setting was subjected to periodic tectonic forcing composed of alternating intervals of tectonic activity and quiescence, both having a duration of 250 kyr (Fig. 5). Although there are no indications from the stratigraphic record that tectonic activity is periodic, it is applied as such in the model in order to facilitate recognition of the related stratigraphic response. The duration of a tectonic pulse is comparable to that of the smaller sequences in the Montanyana Group (Nijman, 1998). The horizontal displacement rate of the thrust fault is 5·0 m kyr^{-1}, which is in the range of average Eocene convergence rates obtained from balanced cross-sections in the Pyrenees (Burbank *et al.*, 1992; Meigs, 1997). The corresponding vertical uplift rate over the thrust ramp dipping at 20° is about 1·82 m kyr^{-1}. The flexural adjustments upon thrust-load emplacement result in a subsidence rate of $\approx$0·23 m kyr^{-1} in the proximal basin area and $\approx$0·15 m kyr^{-1} away from the front of the orogen (Figs 2 and 5a). Oscillations of eustatic sea level with a frequency of 100 kyr and an amplitude of 7·5 m are superimposed on the pulsating tectonic activity (Fig. 5b). Again, the frequency and amplitude are chosen to approximate the small-scale architectural stacking pattern observed in the Montanyana Group (Fig. 1; Nijman, 1998). The eustatic and tectonic components together determine the relative sea-level change and the basin average development of accommodation (Fig. 5c). Many authors suggest that the rate of relative sea-level change rather than the absolute relative sea level is a key factor in controlling the formation of sequence-bounding unconformities and incised valleys (Posamentier & Vail, 1988; Shanley & McCabe, 1994). Relative sea-level change as a function of time is therefore also depicted for comparison with the modelled stratigraphy (Fig. 5d). From this curve, it is clear that the most rapid rises in relative sea level (0·6 m kyr^{-1}) are found during intervals of tectonic activity combined with eustatic rises, whereas the most rapid decreases in relative sea level are limited to eustatic falls during times of tectonic quiescence (−0·5 m kyr^{-1}).

RESULTS

Geomorphic response to tectonic and eustatic change

The main geomorphic processes respond differently to the tectonic and eustatic perturbations

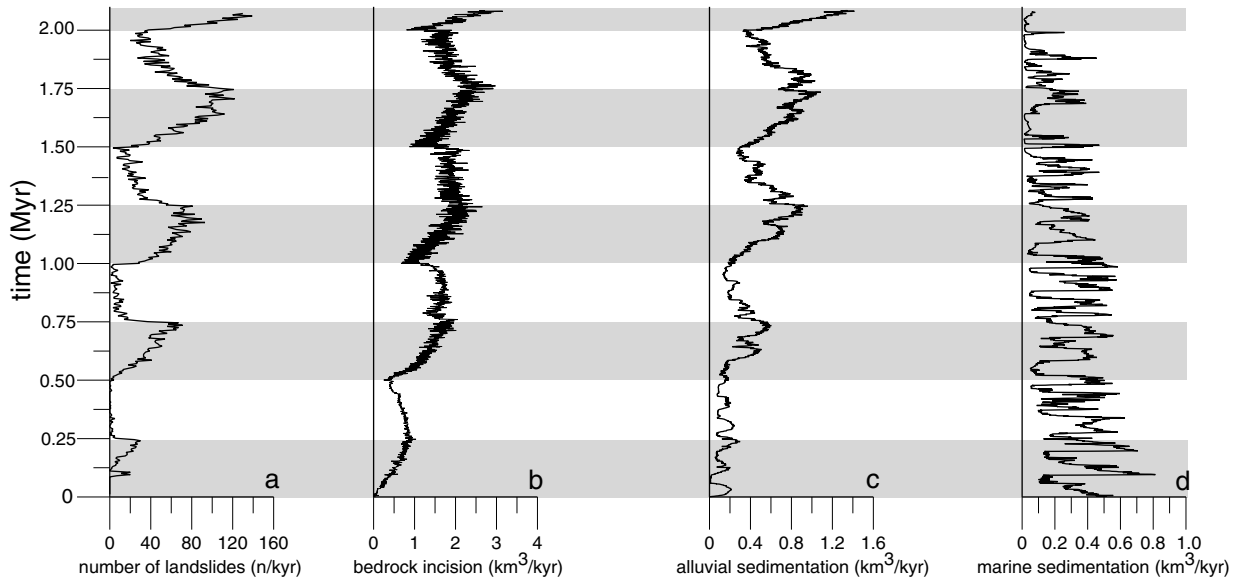

Fig. 6. Response of the main surface processes to the tectonic and eustatic forcing applied. The volumes transported by the different processes are increasingly a function of eustasy whilst the tectonic signal becomes less recognizable. Grey bands represent phases of tectonic activity. See text for discussion.

applied to the model space (Fig. 6a–d). The number of bedrock collapse events shows a good correlation with the history of alternating tectonically active and quiescent intervals. Collapses start after ≈10 kyr because, at the beginning of the run, there is insufficient relief to initiate slide events. Immediately after the first change from tectonic activity to quiescence, the number of collapses in the system is reduced to a few events per kyr. In successive active–quiescent couplets, the distribution of the number of collapse events takes the shape of a typical response curve, with a gradual increase during tectonic activity, followed by a more rapid decline during quiescence (Fig. 6a). The form of these asymmetric response curves changes slightly during the experiment. The maximum number of events rises during successive tectonically active intervals as a result of the cumulative growth in relief of the hanging-wall block. For the first two tectonically active intervals, the maximum number of events coincides with the transition from tectonic activity to quiescence, whereas in the last two active intervals, the maximum is already reached at three-quarters of the way through the pulse. Also, the decrease in events is more gradual during the last quiescence intervals, and the number of events during quiescence rises, reflecting accumulated relief.

The rate of fluvial bedrock erosion is also influenced by the tectonic pulses, but to a lesser degree (Fig. 6b). Again tectonic activity–quiescence couplets correspond to an increase and then a decrease in the eroded volume. The shape of the curve is more symmetrical than that for the collapse events, indicating a more transient response. A notable feature of the curve is the sharp fall directly after the transitions to tectonic activity. Intuitively, a rise might be expected, but the response is explained by interaction with the bedrock collapse events. The sediment liberated by the collapses is distributed through the catchment valleys as mass-flow sheets. Consequently, their sediment temporally blankets the valley floors during (renewed) tectonic activity and protects the bedrock temporarily from exposure and removal by fluvial incision.

The model drainage basin does not reach a mass-based equilibrium, where mass influx and uplift due to thrusting are balanced by erosional removal by surface processes, within the 2·0 Myr of the simulation. The time span needed to reach such an equilibrium with the current values of tectonic uplift and bedrock erodibility approximates 2–4 Myr (Clevis *et al.*, 2003).

The control of sea-level variation on the geomorphic response varies. Neither bedrock collapse events nor bedrock incision are influenced by fluctuations in eustatic sea level (Fig. 6a and b). In order to investigate this quantitatively, both time series were subjected to frequency analysis, but no 100 kyr signal was detected. In contrast to the model results obtained by Humphrey & Heller (1995), there is no evidence that sea level-induced, transient waves of erosion and deposition are transmitted to the catchments. Most likely, the sea-level signal is subdued in the present model because of the high rate of accommodation creation and the large differences between the erodibility of bedrock and alluvial sediment.

The processes operating in the adjacent sedimentary basin are, of course, influenced by the eustatic sea-level fluctuations (Fig. 6c and d). The large-scale, undulating trend in the curve of the volumetric alluvial deposition rate corresponds to the tectonic history and has a similar symmetry to the bedrock incision. Superimposed on the curve are smaller variations, reflecting the eustatic sea-level fluctuation. Responses to the sea-level fluctuations are dominant in the marine deposition curve. Single responses often have a sharp base, followed by a decline reflecting rapid flooding and gradual filling of the new marine accommodation.

Response of the axial-alluvial system to tectonic and eustatic change

The axial-alluvial system in the modelled foreland basin is sensitive to both the tectonic pulses and the eustatic sea-level variations (Fig. 7). During tectonic activity (A), the increase in flexural subsidence causes a rise in the relative sea level and basin-wide retreat of the shoreline (Fig. 7a, c, e and g). Channels on the axial-delta plain respond to the relative sea-level rise by rapid backfilling, with frequent abandonment of positions and splitting of flow in order to spread the carried sediment load as efficiently as possible. Consequently, many short-lived, shallow, braided channels dominate the delta plain, which eventually takes the form of a cone with a convex topography (Fig. 7a, c, e and g) During tectonic quiescence (Q), no accommodation is created by flexural subsidence, and the delta is forced to prograde rapidly in order to keep its preferred equilibrium depositional slope (≈ 0·0025 m m^{-1}; Fig. 7b, d, f and h). Initially, during this forced progradation phase, the system is still covered by many unstable bifurcating channels, and the

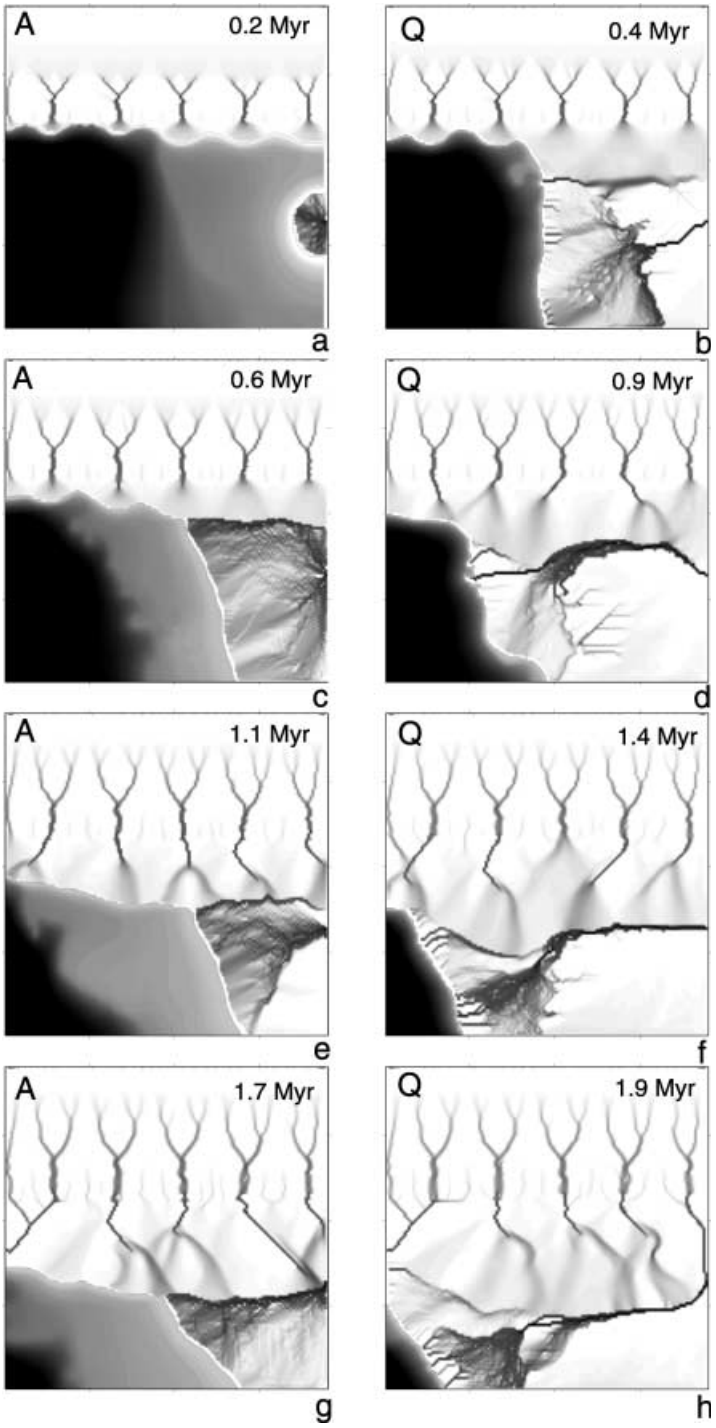

Fig. 7. Time steps in the water discharge patterns of the axial-delta and the alluvial fans draining into the shallow-marine embayment on the foreland. Tectonic phases of active flexural subsidence (A) are characterized by a dominance of distributive channel patterns on the axial-deltaic plain as a result of the rise in relative sea level. During tectonic quiescent (Q) periods, fluvial patterns are more diverse, showing single channels in the proximal deltaic plain. Single channels and funnelling of the flow at the delta front are the result of incision triggered by simultaneous eustatic sea-level lowstands.

surface of the deltaic cone is everywhere close to or approaching its equilibrium slope. As a consequence, the prograding deltaic system is critical with respect to any increases in local water discharge or surface slope.

Increases in local discharge by occasional confluences of streams lead to rapid increases in sediment-carrying capacity that exceed the local sediment load because the discharge exponent m_f in Eq. (1) is chosen higher than unity. The result is incision and the creation of a single feeder channel. A similar phased transition from a bifurcating to a single channel morphology during rapid forced progradation is predicted by Wescott (1993) and is also observed in flume fan experiments (Koss *et al.*, 1994; Bryant *et al.*,

1995; van Heijst & Postma, 2001). As these flume systems experience no subsidence, corresponding to the quiescent conditions simulated here, their behaviour seems to support the choice of m_f used in the model. Another method of triggering channellization during the quiescence phases is the exposure of steep sloping delta front topography across which the delta streams flow during forced progradation, possibly accelerated by emergence of the clinoform breaks by simultaneous eustatic sea-level falls. This is the most common pattern observed in the model, and examples of this are seen in Fig. 7b, d, f and h, where the discharge is funnelled into multiple incised channels close to the coastline. After initialization, the erosion in the coastal channels propagates landward as a set of competing knickpoints heading for the input point for the axial system. A channel capturing the discharge of a competing channel has more chance of connecting first with the inlet and focusing all discharge in an incised trunk channel. The long incised channels present on the upper deltaic plain (Fig. 7b, d, f and h) are the result of previous eustatic lowstands during the quiescence phase. The rate of knickpoint migration within the delta plain streams is dependent on local discharge and sediment load carried by the flow and ranges between 1·0 and 100 myr^{-1}. These rates are in agreement with values derived from Quaternary delta systems (van Heijst & Postma, 2001). The main axial channels preferably form during tectonically quiescent periods in the depression between the fringes of the alluvial fans and the slightly convex delta body, which was shaped by the bifurcating channel pattern during a previous phase of active flexural subsidence (Fig. 7c, d–f).

Foreland basin landscapes

Two snapshots (0·9 Myr and 1·9 Myr) in the development of the modelled foreland basin landscape are shown in Fig. 8. Both landscapes represent eustatic lowstands simultaneous with a phase of tectonic quiescence, but in different stages of filling of the basin. At 0·9 Myr (Fig. 8a), the axial channel is deflected towards the fault front and located in the depression adjacent to the alluvial fan fringes. The morphology of the axial system changes downstream from a single channel through a confined braidplain to a true deltaic distributary system (1, 2 and 3 in Fig. 8a). Two types of response to eustatic fall during quiescence are identified on the alluvial plain. First, small dendritic networks are formed on part of the alluvial plain where the sediment supply is insufficient to dampen the erosive wave (4 in Fig. 8a) triggered by the eustatic fall. Secondly, the delta system reacts by propagation due to the high sediment load. However, a large portion of the water discharge is locally funnelled into a straight channel, suggesting some incision on the deltaic distributary (5 in Fig. 8a). At 1·9 Myr, the marine embayment is almost entirely filled with sediment, and the alluvial fans have prograded further on to the alluvial plain, while their apices show signs of fan-head entrenchment in the proximal regions (1 in Fig. 8b). The transport regime on the fans changes downstream from erosive or bypassing to depositional, and the feeder channels bifurcate while depositing lobes. On the axial-delta plain, the main channel is deflected away from the orogenic front by the progradation of the alluvial fans, but it still shows a preference for a position close to the fan fringes (2 in Fig. 8b). An earlier but now abandoned delta distributary system is found in a downstream direction. The new distributary forms away from the mountain front by a complex of upstream avulsions (3 and 4 in Fig. 8b). Four eustatic lowstand-induced channels, funnelling the drainage to the coastline, mark the new delta front (5 in Fig. 8b).

Basin fill

The modelled basin fill stratigraphy can be visualized as longitudinal and transverse cross-sections (Figs 9 and 10) or as a fence diagram (Fig. 11). Rendered animations of fence diagrams give a good impression of the three-dimensional stratigraphic variability in the synthetic basin fill. However, for a thorough generic analysis, individual cross-sections are preferred because they capture the stratigraphic detail present in the model. The sections are annotated with timelines, which can be drawn at user-defined time intervals, here 50 kyr.

Longitudinal section

A longitudinal stratigraphic section, parallel to the basin axis, is selected to describe the difference between tectonic- and eustatic-dominated sequences (Fig. 9). This section resembles that of a classic prograding delta where the timelines in the alluvial delta-top facies change into shingles of marine clinoforms, and where their inflection point reflects the position of the shoreline (1 and 6 in Fig. 9a). In the top of this section, the advancing alluvial fan deposits are apparent (2 in Fig. 9a).

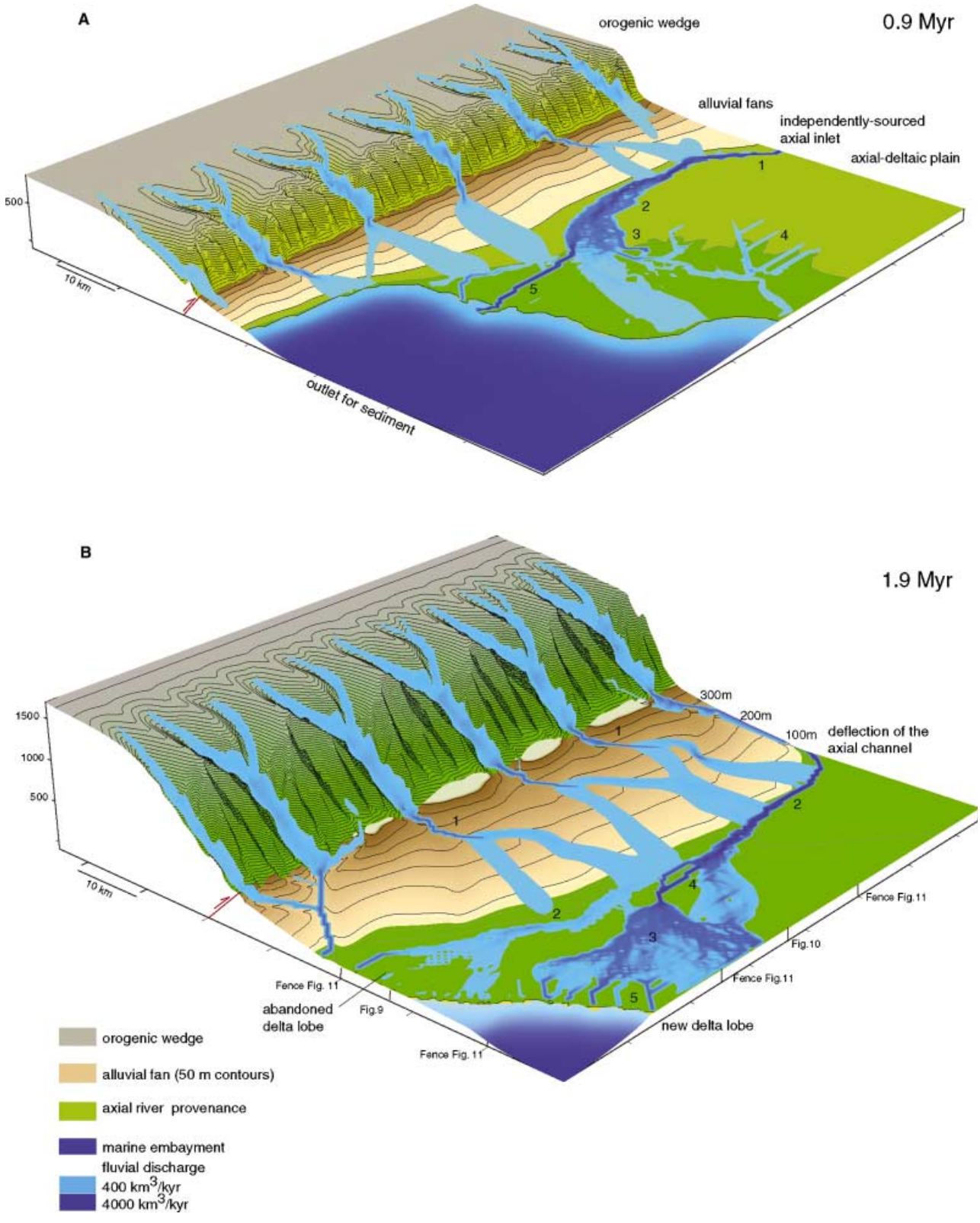

Within this section, two types of axial-deltaic progradational sequence can be distinguished. The first type corresponds to tectonically quiescent (Q) intervals and is characterized by: (1) a large basinward shift of the shoreline position together with superposition of coarse alluvial over fine-grained

Fig. 8. Two examples of the modelled foreland basin landscape at 0·9 Myr (A) and 1·9 Myr (B), during two phases of tectonic quiescence and forced progradation. Both figures show the configuration of the main depositional elements filling the basin; transverse alluvial fans and an axial river discharging into the marine embayment as a delta. The main axial channel has a fixed inlet position but is drawn to the zone of high accommodation creation close to the fan fringes (A). Eventually, the fans deflect this channel basinward (B). Features in (A) discussed in the text are (1) incised axial channel, (2) confined braidplain, (3) deltaic distributary, (4) incision into the upper deltaic plain and (5) incised channel triggered by a eustatic fall, funnelling the bulk of the discharge. Features discussed in (B) are (1) fan head entrenchment, (2) axial channel close to fan fringes, (3) and (4) locations of upstream avulsion leaving a downstream delta abandoned and (5) new delta with juvenile incisions triggered by a eustatic fall. Positions of the stratigraphic cross-sections in Figs 9–11 are indicated along the edges of landscape (B).

sediments (3 in Fig. 9a); (2) entrenchment of the relatively coarse alluvium (4 in Fig. 9a); and (3) coarsening-up trends in the marine delta lobes (5 in Fig. 9a). Three of these progradational sequences are recognizable before the alluvial fan deposits enter the plane of section. The second type of sequence is stacked in between these large-scale progradational sequences. They are deposited during tectonic activity (A) and consist of coarsening-up trends without down-cutting channels, alternated with marine onlap (6 in Fig. 9a).

The signature of eustatic variation on both types of sequences is explored using Fig. 5d and its graphical derivative, Fig. 9c, in which the section is coloured according to the rate of relative sea-level change during deposition of the individual strata. Three individual progradational sequences of the second type are recognized in the base of the section, each corresponding to successive eustatic sea-level lowstands during the first interval of thrusting and related flexural subsidence (0–250 kyr, Fig. 5). Their deposition is synchronous with moderate rates of fall of relative sea-level (1 in Fig. 9c). Periodically, these alluvial plain deposits submerge from a combination of eustatic and subsidence-induced sea-level rise (2 in Fig. 9c). The resulting maximum flooding surfaces are indicated by thin bands of onlapping carbonates, often occupying a position at the clinoform–topset transitions (6 in Fig. 9a). Because the relative sea level does not fall below the clinoform breaks during the deposition of these sequences and, consequently, no fluvial incision is triggered at their boundaries, they resemble type 2 sequences (Van Wagoner *et al.*, 1988).

The channellized delta top progradations are deposited concurrently with or shortly after the most rapid falls in relative sea level (3 in Fig. 9c). They are coeval with tectonically quiescent intervals, which involve a cessation of flexural subsidence and therefore a reduction in the rate of creation of accommodation. As a result, the axial delta is forced to prograde in order to spread the sediment load carried under its preferred equilibrium slope conditions. Fluctuations in the eustatic sea level are no longer compensated by subsidence-induced sea-level rise, and eustatic falls induce the formation of incised channels by knickpoint retreat. Indicative of this incisive, channel-forming process are the reddish colours of the channel lags in the section; their initial fills are coincident with the most rapid falls in relative sea level ($< -0{\cdot}4$ m kyr^{-1}, 4 in Fig. 9c) that occurred well below the clinoform break. Therefore, and because of the grain-size facies dislocation, the horizons of composite incision represent the base of a type 1 sequence (Van Wagoner *et al.*, 1988). So, both progradation types reflect phases of low accommodation but are controlled by a different combination of eustatic oscillation and tectonic subsidence.

Different generations of the axial channel can amalgamate (7 in Fig. 9a) because the approximate channel position is reused during the two cycles of eustatic change during one interval of tectonic quiescence (Fig. 5). Alternatively, channel positions may relocate by increased active bifurcation and avulsion during eustatic sea-level highs, leaving a previously incised channel abandoned and filled with fine-grained, shallow-marine sediments (8 in Fig. 9a). The grain size of the channel fill depends on the relative positions of the successive channels and the cross-section drawn through the synthetic basin fill. Animations depicting the surface drainage evolution and stratigraphic cross-sections indicate that the zone close to the alluvial fan toes offers the best chance of finding a suite of incised, axial channels filled by coarse-grained sediment. This is because, during tectonic quiescence and associated progradation, the axial stream preferably migrates into the topographical depression between the alluvial fan fringes and the slightly convex topography of the axial delta body. Locked in this position and connected to deeper water, the axial channel is very susceptible to incision triggered by simultaneous eustatic lowstands. During these lowstands, most of the

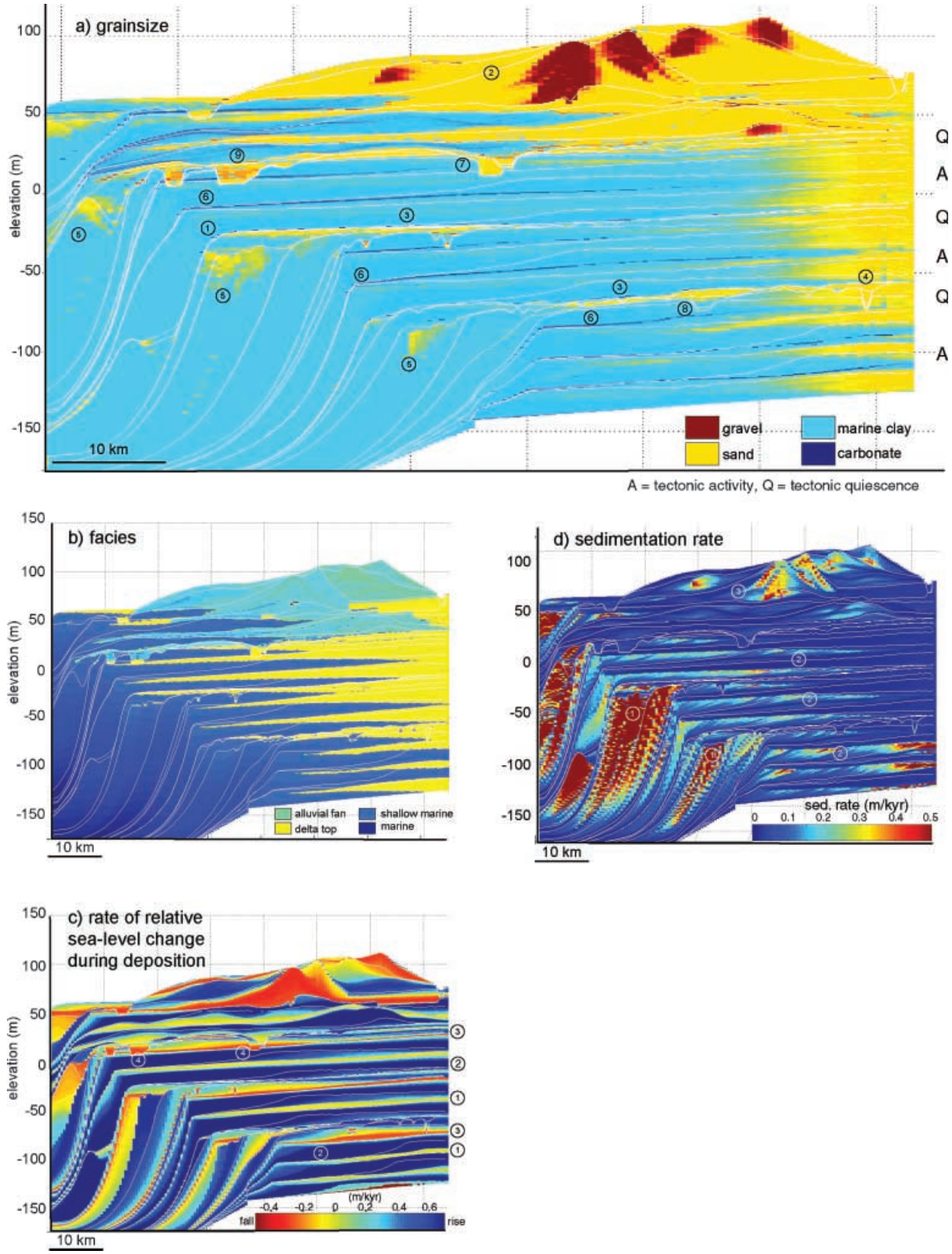

Fig. 9. Longitudinal stratigraphic section through the basin fill dominated by axial-deltaic sediments. Section is coloured according to grain size (a), facies (b), rate of relative sea-level change of the individual strata during their deposition (c) and sedimentation rate (d). Circled numbers identify features discussed in the text. See text for explanation.

sediment load bypasses the alluvial plain and is dumped at high sedimentation rates as delta lobes in marine waters (1 in Fig. 9d and 5 in Fig. 9a). The coarsening-up grain-size trend visible in some of these delta lobes is the result of grain-size sorting by progressive selective deposition (Paola *et al.*, 1992) as these structures build up and emerge (5 in Fig. 9a).

The renewed onset of subsidence during tectonic activity causes active sedimentation to retreat over the rapidly subsiding deltaic plain. Consequently, the delta lobes starve and become covered by a thin sheet of carbonate. During the syntectonic falls in eustatic sea level that follow, the axial system periodically progrades, showing a foreset-like pattern in the sedimentation rate cross-section (2 in Fig. 9d). The foreset pattern is the result of the frequent relocation of axial channels due to the filling of local accommodation at the coastline. Eventually, transverse alluvial fan lobes bury the delta plain (2 in Fig. 9a). The incised valleys, previously created by the delta streams, are in places used and laterally filled by the advancing alluvial fan lobes. Coarse alluvial fan sediment is visible in the incised valleys 9 and 7 in Fig. 9a, covering an initial fill of axial-deltaic provenance. The alluvial fan lobes are marked by radial decreasing grain sizes and sedimentation rates (2 in Fig. 9a and 3 in Fig. 9d). Delta flows curving around the fan bodies result in intercalated patches of delta sediment in between the fan bodies (Fig. 9b) while both systems are competing for the same zone of high accommodation, especially during tectonic quiescence.

Thrust-perpendicular section

In the section perpendicular to the strike of the thrust front, the basin is asymmetric as a result of the differential subsidence rate across the basin, which increases towards the thrust fault (Fig. 10). The stratigraphic patterns indicated by the timelines in the basin centre show a transition from lobate to tabular stratification. This transition from marine delta lobe clinoforms to horizontal delta tops reflects the decrease in accommodation at the location of the section as a result of the progressive infilling of the basin with sediment. In the lower half of the section, coarse-grained sediment is only found in the tops of lobes or in the incised channels (1 in Fig. 10a). The upper half of the section is marked by intercalations of sandier, channellized alluvium with fine-grained sediment and carbonate onlaps, reflecting the eustatic sea-level fluctuations.

Coalescing alluvial fans form a bajada that is marked by a continuous but indented progradation of gravel and sand into the basin. The small-scale expansion and retreat patterns of the fans (2 in Fig. 10a) are the result of the successive eustatic sea-level falls and rise, while the large fan progradations occur during intervals of tectonic quiescence (3 in Fig. 10a). The main reason for fan progradation is the decrease in accommodation during quiescence, a response similar to that of the axial delta. Both depositional systems compete during quiescent phases for the limited accommodation close to the fault front. Coeval axial stream patterns preferably follow the basin axis and occasionally trim the fan toes, which is visible stratigraphically as a steepening and merging of the fan timelines (encircled in Fig. 10d).

The alluvial fans tend to react more slowly to a decrease in accommodation than the axial system, because they are able to store sediment below their steeper sloping fluvial profiles. Consequently, they prograde slightly later and overlie the axial alluvium, which is initially deposited close to the thrust front during the start of a quiescence interval (see inset of the fence diagram Fig. 11).

The detached gravel bodies visible in Figs 10 and 11 represent secondary fan lobes, deposited midway down the bajada, downstream of the locations where the fan streams bifurcate and lose their transport capacity rapidly (Fig. 8b, downstream of 1). As a result of the preferential deposition mechanism in the perfect sorting algorithm applied, these lobes are enriched in gravel during their aggradation. Some lobes even have a mushroom shape with an entrenched channel at their base (Fig. 11). This is the result of progressive backfilling of a fan channel by the lobe, while the stream is bifurcating around the lobe itself. This self-sustaining process is interrupted as the lobe migrates on to the steeper parts of the bajada, and all discharge is deflected along one side of the lobe.

Three-dimensional visualization of subsurface channel belts

In order to illustrate the potential of forward models for applied reservoir studies, a second basin-filling experiment by transverse and axial sources was conducted, focusing on the analysis and visualization of the main axial-channel stacking pattern (Fig. 12). The scenario modelled consisted of 400 kyr tectonic pulses and a

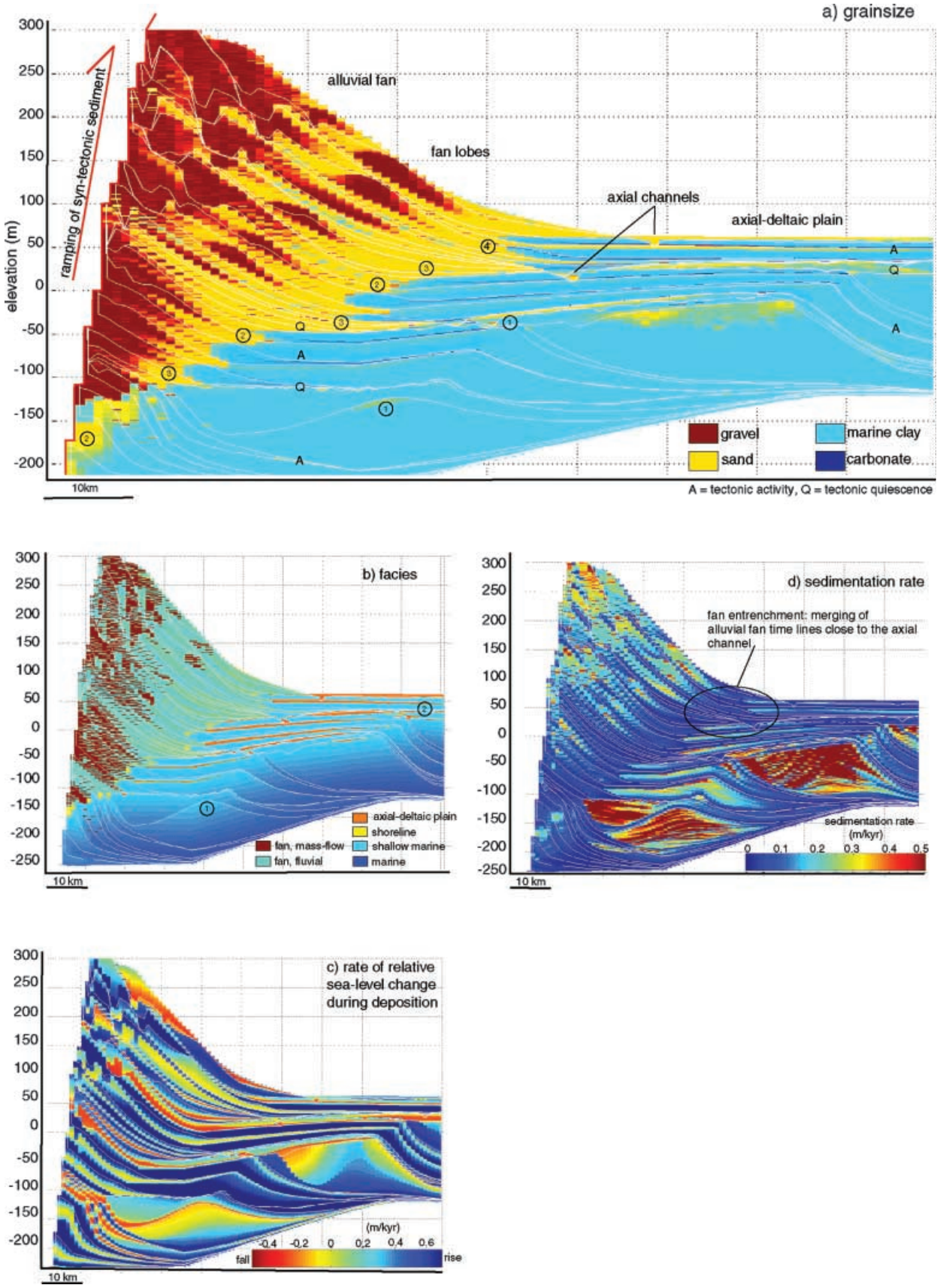
a) grainsize
alluvial fan
fan lobes
axial channels
axial-deltaic plain
ramping of syn-tectonic sediment
elevation (m)
gravel
sand
marine clay
carbonate
A = tectonic activity, Q = tectonic quiescence
10km
b) facies
axial-deltaic plain
shoreline
shallow marine
marine
fan, mass-flow
fan, fluvial
10 km
d) sedimentation rate
fan entrenchment: merging of alluvial fan time lines close to the axial channel
sedimentation rate (m/kyr)
0 0.1 0.2 0.3 0.4 0.5
10 km
c) rate of relative sea-level change during deposition
(m/kyr)
-0.4 -0.2 0 0.2 0.4 0.6
fall
rise
10 km

Fig. 10. Stratigraphic section through the basin fill perpendicular to the thrust fault. Section is coloured according to grain size (a), facies (b), rate of relative sea-level change of the individual strata during their deposition (c) and sedimentation rate (d). Circled numbers identify features discussed in the text. See text for explanation.

high-frequency sea-level fluctuation of 40 kyr in order to create multiple incised channels. These 40 kyr sea-level oscillations are rare in the sedimentary record, but they are inferred, for example, from the Quaternary foreland basin deposits of Taiwan (Chen *et al.*, 2001) where their preservation in the stratigraphy is facilitated by high rates of subsidence and sediment supply.

After 2·5 Myr of simulation time, the axial channel strata are selected from the three-dimensional synthetic stratigraphic data set and visualized using two criteria. First, they have to be deposited by the axial system at water discharge conditions that approximate the discharge of the axial inlet cell. Secondly, they contain more than 50% sand. The resulting three-dimensional distribution of coarse-grained channel voxels delineates the successive positions of the main axial-deltaic channel belt in the subsurface (Fig. 12; see *Supplementary material*). Three channel belt horizons are visible, all corresponding to periods of axial-delta progradation resulting from limited accommodation generation during phases of tectonic quiescence: (1) 0·4–0·8 Myr; (2) 1·2–1·6 Myr; and (3) 2·0–2·4 Myr. They originate from a vertical stack of voxels at the left-hand side of the figure that indicates the location of the fixed inlet cell of the axial system (Fig. 2). The lower channel belt is relatively thick ($\approx$ 20 m) but thins distally towards the marine embayment by branching. These distributaries are the result of successive deflections of the axial streams resulting from the emergence and obstruction by offshore delta lobes. Chronologically, the individual branches young towards the foreland because the obstructing lobes fill up the high-subsidence zone close to the thrust fault first, and then relocate to a more basinward position as the accommodation close to the fault front is filled up (see *Supplementary material* associated with Fig. 12). The second and third channel belts are progressively located in a more basinward position, but this is caused by the obstruction of the entire axial system by the continuous progradation of the alluvial fans.

DISCUSSION

The high-resolution model of foreland basin filling presented here resembles that of a natural foreland basin in three ways (Bentham *et al.*, 1992; Nijman, 1998; Remacha *et al.*, 1998; Ramos *et al.*, 2002). First, the basin is progressively filled by an axial delta as a result of the long-term dominance of clastic supply over the accommodation created, causing a regression (Bentham *et al.*, 1992; Remacha *et al.*, 1998). Secondly, the final stratal patterns have a wedge-shaped geometry due to the asymmetrical generation of accommodation by flexural subsidence, just as in natural foreland basins.

Thirdly, transverse alluvial fans become more important as a source of clastics with time, and they push away the axial system and bury the sediments previously deposited by the axial-delta during the transition to the overfilled basin phase (cf. Brozovic & Burbank, 2000). This is well known from the stratigraphy of the Pyrenean foreland basin, where Early Miocene terminal fan systems cover Eocene axial-deltaic deposits (Hirst & Nichols, 1986; Ramos *et al.*, 2002). In the Alpine foreland basin, the fan expansion is explained by an increase in transverse sediment flux as erosion catches up with uplift during a slowdown or cessation of tectonic convergence after a phase of high shortening rates (Sinclair & Allen, 1992; Schlunegger *et al.*, 1997). The model shows the same non-equilibrium between uplift and erosion, using average values for the shortening and erosional processes and, consequently, a delayed increase in transverse sediment flux. Dynamic equilibrium between uplift and erosion establishes in the model at timescales larger than 2·0 Myr (Clevis *et al.*, 2003). In the present model, this state is difficult to reach due to computational limitations. The distal position of the shifting axial system in the model is bound by the small size of the computational grid. In natural foreland basins, the axial system relocates in a more basinward position, following the length axis of the widening flexural depression (Puigdefàbregas & Souqet, 1986; Jin *et al.*, 1995).

One of the fundamental issues addressed in this model study is the temporal variation of transverse gravel advance in foreland basins. The initial advance of fan gravels in foreland basins is a direct function of the interaction between proximal accommodation generation and the increasing orogenic supply from nearby catchments. In this early phase, vertically stacked fan

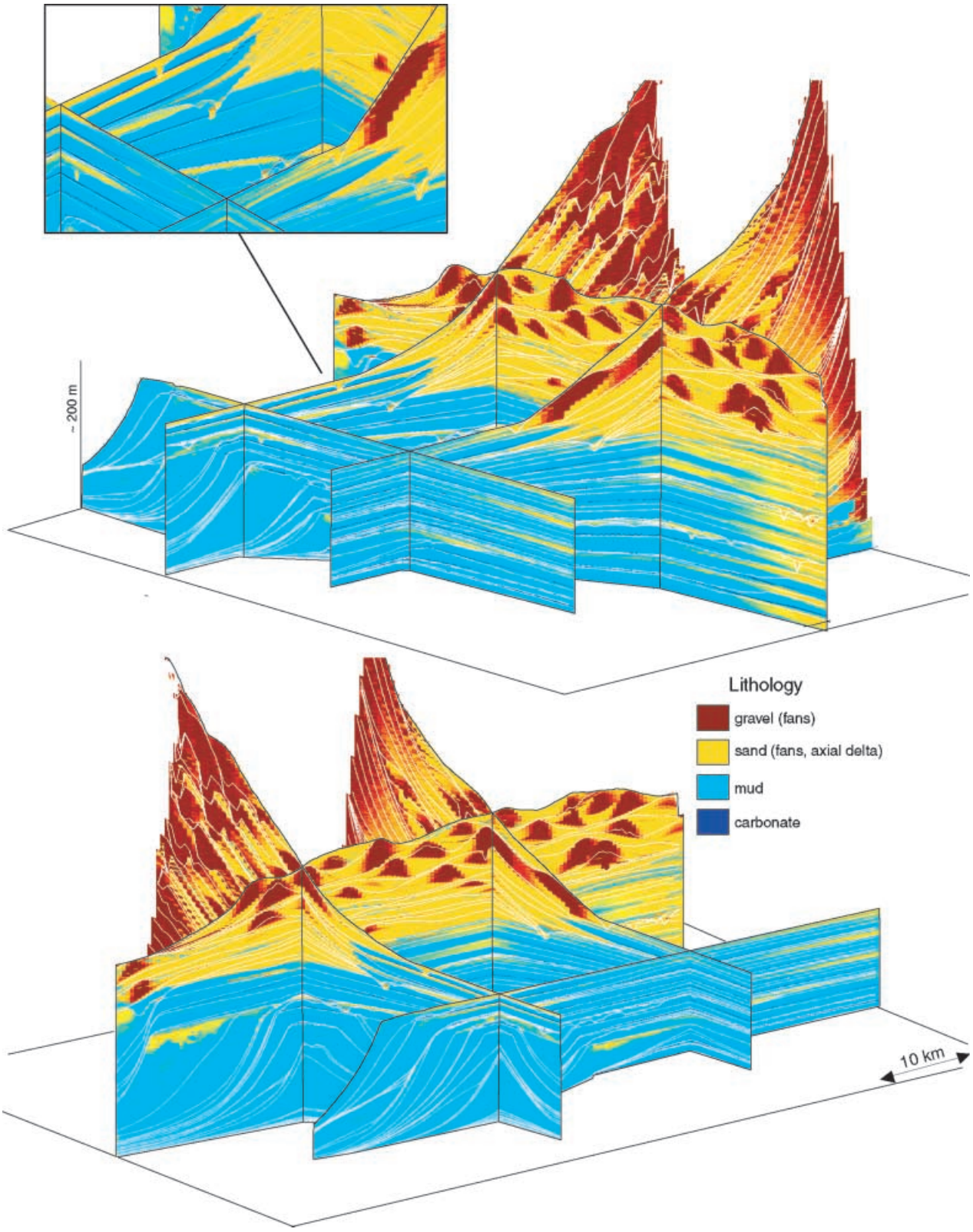

(delta) bodies, reflecting the balance between both components, will dominate the basin fill. However, in a following, overfilled basin stage, care should be taken in interpreting the stratigraphic pattern directly in terms of competing local flexural accommodation and orogenic sup-

Fig. 11. Fence diagram of the foreland basin fill coloured according to lithology viewed from two different angles. Timelines (in white) are spaced at 50 kyr. Alluvial fan gravel and sand are clearly recognizable as the stacked lobate bodies. They progressively cover the axial-deltaic deposits as part of their general progradation. Thin, near-horizontal delta-top sheet sandstones alternating with shallow-marine clays and thin carbonates represent axial-deltaic deposits. Incised channels mark widespread progradations of these sandy delta-top horizons during phases of tectonic quiescence, together with simultaneous deposition of coarsening-up offshore lobes. The inset shows the covering of incised axial channels by alluvial fan toe sands during a phase of tectonic quiescence. This is indicative of the differential response times of both systems upon reduction of accommodation.

ply. The externally sourced axial system is volumetrically an important component in filling the local accommodation, and its supply is most probably unrelated to the intensity of tectonic activity at this position. Consequently, axial-induced overfill and conditions of constant local supply/subsidence could cause fan progradation to accelerate, resulting in thin gravel sheets in the distal foreland without any change in tectonic activity.

The long-term rate of gravel advance in the modelled basin fills is 100–150 m kyr^{-1}, which is relatively high compared with natural fan gravels deposited under similar subsidence rates (Tremp Basin, 40 m kyr^{-1}; Nijman, 1998). This is partly due to the rapid infilling of the basin by axial sediments but also the result of the technique that was used to simulate thrusting in the model. From several synthetic sections, it is concluded that this horizontal component in the tectonic displacement contributes 20% to the long-term fan gravel propagation rate.

The thrusting algorithm used incorporates active ramping or over-riding of syntectonic sediment. Consequently, bedrock-floored fan apices get reworked while the drainage basin outlets increase in elevation. Outlets propagate with the fault trace, and the alluvial fan stream profiles are forced to relocate basinward (Figs 10 and 11). Many conceptual models and numerical analyses of basin filling (Paola *et al.*, 1992; Johnson & Beaumont, 1995) neglect this obvious component in their explanations of gravel progradation, although it is an important contributing factor.

Pulsating tectonic activity in the model results in a pattern of repetitive alluvial fan retreat and advance, where the latter corresponds to phases of tectonic quiescence (Paola *et al.*, 1992), in agreement with other forward model studies of gravel dispersal in foreland basins. The onset of tectonic activity is marked by retrogradation of gravels and onlap of finer grained marine or axially sourced sediment on to the fan surfaces. Syntectonic alluvial fan bodies show a higher density of landslide- over streamflow-deposited strata (Fig. 10b) due to the good correlation of bedrock collapse events with the phases of active tectonic uplift (Fig. 6a). Together with fan retreat and transitions in clast provenance, this is probably a diagnostic feature of active uplift and (re)juvenation of source terrains (Heller & Jones, 2001).

The model has been shown to be able to simulate a hierarchical sequence stacking arrangement of the axial-deltaic system by simultaneously applying phased tectonic activity and eustatic sea-level fluctuations. Many authors have identified such hierarchical arrangements in the stacking of sequences and facies patterns in the shallow-marine to deltaic deposits of foreland basins (Plint, 1991; Nijman, 1998; Dreyer *et al.*, 1999; Chen *et al.*, 2001). The model results illustrate a possible mechanism and the diagnostic features of the sequences and their unconformities. The synthetic 100 kyr sequences, which are controlled by eustatic sea level in the model, lack basal incision when deposited during active tectonic phases. Type 2 sequences are developed as a result of the simultaneous subsidence component in the relative sea-level curve that causes falls in eustatic sea level to be suppressed, so the shoreline does not fall below the clinoform breaks. The type 2 sequence boundaries are hard to recognize in the model, although the consequent carbonate onlaps corresponding to syntectonic eustatic sea-level highs are well developed. Therefore, carbonate onlaps are better markers for delineation of sequences deposited in high-subsidence rate foreland basins as a result of high-frequency sea-level variations. In high-latitude basins, these onlapping sediments could be argillaceous or carbonaceous, if coals occur on the delta top.

The embedded eustatic signal results in a more complex stratigraphic architecture during tectonically quiescent phases when limited accommodation inhibits their preservation in the stratigraphy as complete stacked progradational cycles. Major progradation of the shoreline and delta top facies occurs during quiescence but is punctuated by phases of basal incision as a result of simultaneous eustatic sea-level lowstands. The resulting unconformity is defined by

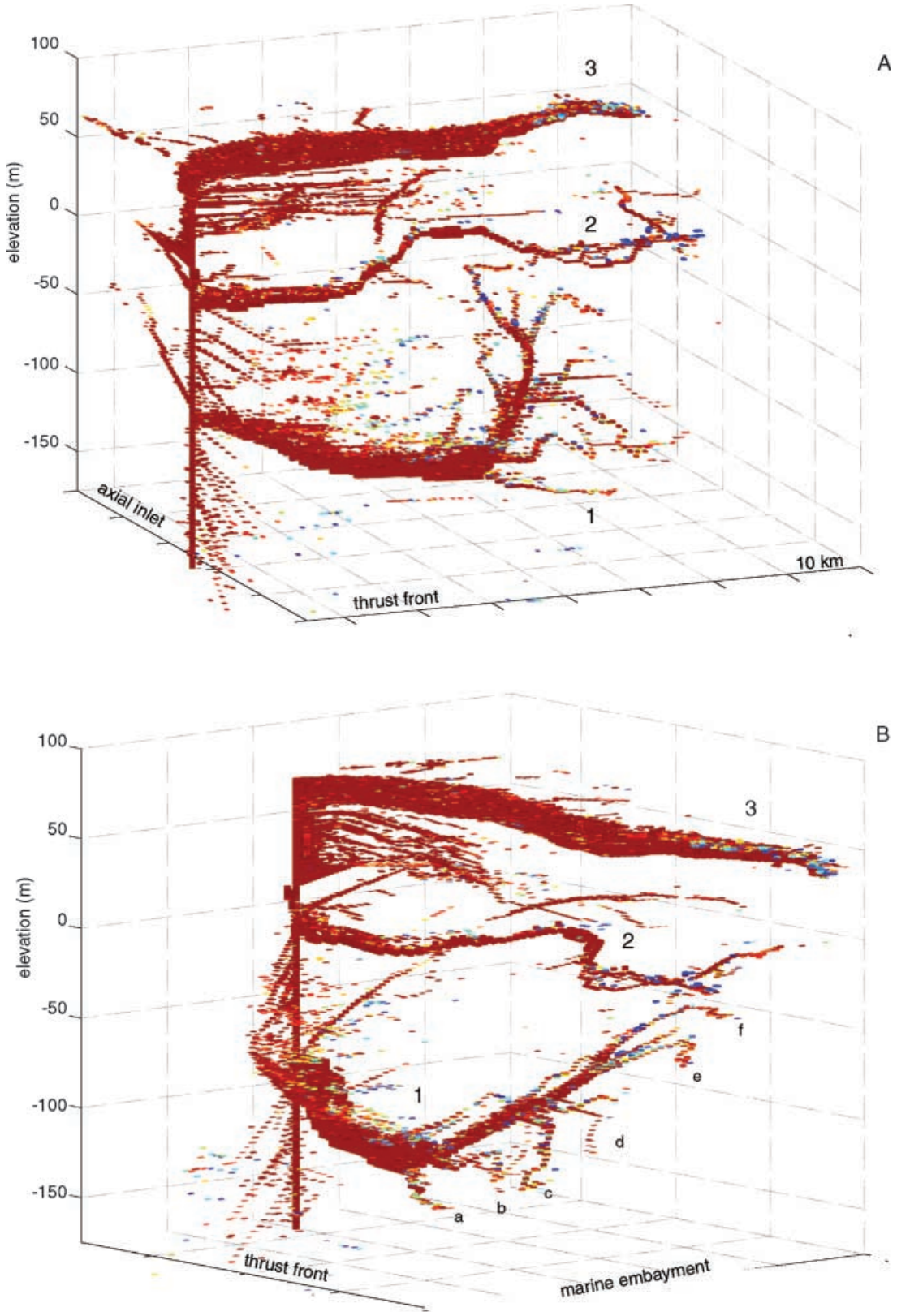

these incised channels and appears in cross-section to be similar to the type 1 sequence boundaries of the classic Exxon model of sequence stratigraphy (Van Wagoner *et al.*, 1988; Emery & Myers, 1996). Note that the unconformities in the model are of composite origin,

Fig. 12. Changing subsurface position of the main channel belt deposited by the axial-deltaic system. Three channel belts are recognizable (1, 2 and 3), all formed during tectonic quiescence phases of low accommodation generation. They are situated spatially between dominantly fine-grained sediments corresponding to phases of higher subsidence rates during tectonic activity. The upper channel belts are successively displaced basinward with respect to the lower one because of the progradation of the alluvial fan front (Fig. 8B). Multiple deflections and branching of the lower channel belt (a–f) are the result of progressive basinward deflection of axial streams as proximal accommodation is filled. See *Supplementary material*.

generated by multiple sea-level lowstands. Furthermore, the resulting unconformity surfaces are discontinuous because their intensity is dependent on the distance to the incising axial-deltaic channel. Therefore, they are of limited value in distinguishing the large-scale sequences or putting exact time constraints on boundaries. The major flooding surfaces, as a result of renewed tectonic activity and subsidence, are more useful because of their basin-wide character and rapid development (e.g. Galloway, 1989). In the model, carbonate sediments indicate the flooding surfaces but, in high-latitude basins, sediments of similar significance are delta top coals or onlapping argillaceous sediments.

The current model does not take into account a more realistic visco-elastic flexural response to thrust loading. Incorporating this would retard the accommodation effects related to tectonic pulsation by 10–20 kyr. After cessation of tectonic activity, subsidence would continue and decrease gradually, whereas during the start of a tectonic phase, subsidence rates would increase steadily. However, the lack of a more sophisticated flexure model does not invalidate the results presented, as the modelled tectonic pulses have a duration 10 times longer than the visco-elastic response time.

The overall stratigraphic architecture generated by the model is similar to the observed architecture in the Lower Montanyana Group of the Tremp Basin (Figs 1 and 9a), suggesting that a combination of changing tectonic accommodation and eustatic sea-level fluctuations might explain the patterns observed in the Lower Montanyana Group. The high-frequency cycles of axial-deltaic progradation lacking incision are very similar, and the retreating alluvial fans and stagnant axial delta during the ULM sequence could reflect a phase of tectonically enhanced subsidence. The pronounced quiescence progradations shown by the model are less evident in Fig. 1c, except for the LLM-3 and the Mid-Montanyana (MM) Castissent sequence. The outcrop pattern observed suggests a more gradual decrease in accommodation during the transition between the LLM and ULM instead of a true quiescence phase. The forced regression of the MM Castissent sequence is of the type observed in the model scenario. However, there is a more complex tectonic mechanism proposed to explain the reduced accommodation during the deposition of the MM sequence such as the activity of a subsurface detachment fault beneath the basin. The stratigraphic implications of this structure are explored elsewhere (Clevis *et al.*, in press).

Axial channel belts are sediment bodies of high reservoir potential in foreland basins, and the model allows for the visualization of their subsurface structure. Generally, their position follows the zone of maximum accommodation between the alluvial fan fringes and the convex topography of the axial delta. This zone is relocated away from the tectonic front as the alluvial fans prograde and obstruct the axial system. However, in order to investigate the model's predictive capabilities, several channel belt locations, generated in more than one model experiment, should be evaluated statistically. Exact channel positions vary slightly throughout multiple runs under conditions of identical model input because of internal random behaviour of the cellular model approach (cf. Meijer, 2002).

CONCLUSIONS

This study shows that it is possible to capture the basic tectono-geomorphic evolution and simultaneous filling of a proximal foreland basin by independent axial and transverse sediment sources in a three-dimensional forward numerical model. The synthetic stratigraphy is of high resolution when compared with existing foreland basin models and can be coloured according to the rate of relative sea-level change, facilitating correlation of the stratigraphic architecture with the external forcing. A combination of variable tectonic activity and a superimposed eustatic sea-level oscillation produces a hierarchical stacking pattern of axial-deltaic and alluvial fan sequences separated by thin carbonate onlapping deposits and unconformities, patterns that are characteristic of many natural foreland basins.

The basic controlling mechanism behind the large-scale stacking of these sequences is the balance between supply and flexurally created accommodation. Owing to the elastic flexure solution applied and the character of the sediment supply to the axial-delta and alluvial fans, alternating phases of tectonic activity and quiescence lead to retrogradation and progradation of both systems. Syntectonic eustatic sea-level fluctuations result in a set of parasequence-scale packages of prograding and shallowing-upward deltaic sediments bounded by type 2 sequence boundaries. Incised channels are rare within these sequences but are characteristic features of tectonically quiescent phases where eustatic falls are no longer dampened by subsidence. Suites of amalgamating, axial channels mark the resulting type 1 sequence boundaries. Coarse-grained incised channel fills are formed preferentially in the zone of maximum accommodation between the alluvial fan fringes and the slightly convex topography of the axial delta. These potential reservoir bodies can easily be extracted from the synthetic subsurface volume and visualized in three dimensions, illustrating an application of stratigraphic forward modelling in foreland basin settings.

ACKNOWLEDGEMENTS

We are grateful to Greg Tucker (Oxford University, UK) for providing his GOLEM surface processes code, which was used as a basis in the construction of this stratigraphic foreland basin model. Dave Waltham, Peter Haughton and an anonymous reviewer are thanked for their constructive comments, which helped to improve the manuscript.

SUPPLEMENTARY MATERIAL

The following material is available from http://www.blackwellpublishing.com/products/journals/suppmat/sed/sed652/sed652sm.htm

Fig. S1. Animation showing the three-dimensional structure in a 360° rendering of the channel fills.

NOMENCLATURE

Δx, δx, δy Spatial discretization of the landscape surface (500 m)

Δt Time step size for geomorphic processes (10 years)

W Local channel width (m, approximated as $\approx Q^{0.5}$),

Q Local water discharge ($m^3\ yr^{-1}$)

S Local slope (–)

$K_{f\ axial\ delta}$ Axial fluvial transport coefficient ($0{\cdot}1\ m^{-3/2}\ yr^{1/2}$)

$K_{f\ alluvial\_fans}$ Alluvial fan fluvial transport coefficient ($0{\cdot}01\ m^{-3/2}\ yr^{1/2}$)

m_f, n_f Fluvial transport capacity exponents (3/2 and 1·0)

K_b Bedrock erodibility coefficient ($1{\cdot}0 \times 10^{-4}$ $year^{-2/3}$)

m_b, n_b Bedrock erodibility exponents (2/3 and 1/3)

R Basin-wide uniform rainfall rate ($1\ myr^{-1}$)

$R_{regolith}$ Bedrock weathering rate ($1{\cdot}0 \times 10^{-5}$ myr^{-1})

θ_c Bedrock collapse critical angle (30°)

θ Potential failure plane dip (°)

C Bedrock effective cohesion ($6 \times 10^4\ kg\ m^{-1}\ s^{-2}$)

β Local hillside slope (> 30°)

ϕ Material friction angle (30°)

H Height above receiving fluvial cell (m)

H_c Critical height (m)

$P_{collapse}$ Bedrock collapse probability (0–1)

K_{marine} Depth-dependent marine diffusion coefficient ($0{\cdot}1\ km^3\ kyr^{-1}$)

P_{carb} Carbonate production rate (0–0·1 m kyr^{-1})

α Thrust ramp (20°)

R_{thrust} Horizontal velocity of the orogenic wedge ($5\ m\ kyr^{-1}$)

EET Effective elastic thickness of the lithosphere (15 km)

REFERENCES

Allen, J.R.L. (1965) A review of the origin and characteristics of recent alluvial sediments. *Sedimentology*, **5,** 89–191.

Anderson, R.S. and **Humprey, N.F.** (1990) Interaction of weathering and transport processes in the evolution of arid landscape. In: *Quantitative Dynamic Stratigraphy* (Ed. T.A. Cross), pp. 349–361. Prentice Hall, Englewood Cliffs.

Baltzer, F. and **Purser, B.H.** (1990) Modern alluvial fan and deltaic sedimentation in a foreland tectonic setting: the Lower Mesopotamian Plain and Arabian Gulf. *Sed. Geol.*, **67,** 175–197.

Bentham, P. and **Burbank, D.W.** (1996) Chronology of the Eocene Foreland Basin Evolution along the Western Oblique Margin of the South-Central Pyrenees. In: *Tertiary Basins of Spain, the stratigraphic record of Crustal Kinematics* (Ed C.J. Dabrio), pp. 144–152. Cambridge University Press, Cambridge.

Bentham, P.A., Burbank, D.W. Puigdefàbregas, C. (1992) Temporal and spatial controls on the alluvial architecture of an axial drainage system: late Escanilla Formation, southern Pyrenean Foreland basin, Spain. *Basin Res.* **4,** 335–352.

Bhattacharya, J. (1991) Regional to sub-regional facies architecture of river-dominated deltas, Upper Cretaceous Dunvegan Formation, Alberta sub-surface. In: *The Three-Dimensional Facies Architecture of Terrigenous Clastic Sediments and its Implications for Hydrocarbon Discovery and Recovery* (Eds A.D. Miall and N. Tyler), *Soc. Sed. Geol. Spec. Publ. 'Concepts and Models in Sedimentology and Paleontology'*, **3,** 189–206.

Bierman, P.R. (1994) Using *in situ* produced cosmogenic isotopes to estimate rates of landscape erosion, a review from the geomorphic perspective. *J. Geophys. Res.*, **99,** 13885–13896.

Blair, T.C. (1999) Alluvial fan and catchment initiation by rock avalanching, Owens Valley, California. *Geomorphology*, **28,** 201–221.

Blair, T.C. and **Bildeau, W.** (1988) Development of tectonic cyclothems in rift pull-apart and foreland basins: sedimentary response to episodic tectonism. *Geology*, **16,** 517–520.

Boscher, H. and **Schlager, W.** (1992) Computer simulation of reef growth. *Sedimentology*, **39,** 503–512.

Brozovic, N. and **Burbank, D.W.** (2000) Dynamic fluvial systems and gravel progradation in the Himalayan foreland. *GSA Bull.*, **112,** 394–412.

Bryant, M., Falk, P. and **Paola, C.** (1995) Experimental study of avulsion frequency and rate of deposition. *Geology*, **23,** 365–368.

Burbank, D.W., Verges, J., Muñoz, J.A. and **Bentham, P.** (1992) Coeval hindward- and forward imbricating thrusting in the south-central Pyrenees, Spain: timing and rates of shortening and deposition. *GSA Bull.*, **104,** 3–17.

Burgess, P.M. and **Hovius, N.** (1998) Rates of delta progradation during highstands: consequences for the timing of deposition in deep-marine systems. *J. Geol. Soc. London*, **155,** 217–222.

Chen, W.S., Ridgway, K.D., Horng, C.S., Chen, Y.G., Shea, K.S. and **Yeh, M.G.** (2001) Stratigraphic architecture, magnetostratigraphy and incised-valley systems of the Pliocene-Pleistocene collisional marine foreland basin of Taiwan. *GSA Bull.*, **113,** 1249–1271.

Clevis, Q. (2003) *Three-dimensional modelling of thrust-controlled foreland basin stratigraphy*. PhD Thesis, Utrecht University, Faculty of Earth Sciences. Geol. Ultraiect., **226,** 136.

Clevis, Q., de Boer, P.L. and **Wachter, M.** (2003) Numerical modelling of drainage basin evolution and three-dimensional alluvial fan stratigraphy. *Sed. Geol.*, **163,** 85–110.

Clevis, Q., de Jager, G., Nijman, W. and **de Boer, P.L.** (2004) Stratigraphic signatures of translation of thrust-sheet top basins over low-angle detachment faults. *Basin Res.*, **16,** 145–163.

Crave, A. and **Davy, P.** (2001) A stochastic 'precipitation' model for simulating erosion/sedimentation dynamics. *Comp. Geosci.*, **27,** 815–827.

De Boer, P.L., Pragt, J.S.J. and **Oost, A.P.** (1991) Vertically persistent sedimentary facies boundaries along growth anitclines and climatic control in the thrust-sheet-top south Pyrenean Tremp-Grauss foreland basin. *Basin Res.*, **3,** 63–78.

Demicco, R.V. (1998) Cycopath 2D – A two-dimensional, forward model of cyclic sedimentation on carbonate platforms. *Comp. Geosci.*, **24,** 405–423.

Densmore, A.L., Ellis, M.A. and **Anderson, R.S.** (1998) Landsliding and the evolution of normal fault bounded mountains. *J. Geophys. Res.*, **103,** 15203–15219.

Dreyer, T., Falt, L.-M., Hoy, T., Knarud, R., Steel, R. and **Cuevas, J.-L.** (1993) Sedimentary architecture of field analogues for reservoir in formation (SAFARI): a case study of the fluvial Escanillia Formation, Spanish Pyrenees. In: *The Geological Modelling of Hydrocarbon Reservoirs and Outcrop Analogues* (Eds S.S. Flint and I.D. Bryant), *IAS Spec. Publ.*, **15,** 57–80.

Dreyer, T., Corregidor, J., Arbues, P. and **Puigdefàbregas, C.** (1999) Architecture of the tectonically influenced Sobrarbe deltaic complex in the Ainsa Basin, northern Spain. *Sed. Geol.*, **127,** 127–169.

Emery, D. and **Myers, K.J.** (1996) *Sequence Stratigraphy*. Blackwell Science, Oxford, 297 pp.

Flemings, P.B. and **Jordan, T.E.** (1990) Stratigraphic modelling of foreland basins; Interpreting thrust deformation and lithosphere rheology. *Geology*, **18,** 430–434.

Galloway, W.E. (1989) Genetic stratigraphic sequences in basin analysis; architecture and genesis of flooding surfaces bounded depositional units. *AAPG Bull.*, **73,** 125–142.

Garcia-Castellanos, D. (2002) Interplay between lithospheric flexure and river transport in foreland basins. *Basin Res.*, **14,** 89–104.

Garcia-Castellanos, D., Fernandez, M. and **Torne, M.** (1997) Numerical modelling of foreland basin formation: a program relating thrusting, flexure, sediment geometry and lithosphere rheology. *Comp. Geosci.*, **23,** 993–1003.

Gawthorpe, R., Hardy, S. and **Ritchie, B.D.** (2003) Numerical modelling of sedimentation in half graben settings. *Sedimentology*, **50,** 169–185.

Geddes, A. (1960) The alluvial morphology of the Indo-Gangetic plain, Its mapping and geographical significance. *Trans. Inst. Br. Geogr.*, **28,** 253–276.

Gupta, S. (1997) Himalayan drainage patterns and the origin of fluvial megafans in the Ganges foreland basin. *Geology*, **25,** 11–14.

Hardy, S. and **Gawthorpe, R.** (2002) Normal fault control on sediment supply to extensional basins: insights from numerical modelling: insights from numerical modelling. *J. Geophys. Res.*, **107,** 2246. DOI: 10.1029/2001JB000166.

Hardy, S. and **Poblet, J.** (1995) The velocity description of deformation. Paper 2: Sediment geometries and fault-bend folding. *Mar. Petrol. Geol.*, **12,** 165–176.

van Heijst, M.W.I.M. and **Postma, G.** (2001) Fluvial response to sea-level changes; a quantitative analogue experimental approach. *Basin Res.*, **13,** 269–292.

Heimsath, A.M., Dietrich, W.E., Nishiizumi, K. and **Finkel, R.C.** (1997) The soil production function and landscape equilibrium. *Nature*, **388,** 358–361.

Heller, P.L. and **Jones, M.A.** (2001) Time lag of syntectonic indicators in foreland basin deposits. In: *AAPG Ann. Meeting Abstract*. AAPG, Denver, CO.

Heller, P.L., Angevine, C.L. and **Wilson, N.S.** (1988) Two phase stratigraphic model of foreland basin sequences. *Geology*, **16,** 501–504.

Hirst, J.P.P. and **Nichols, G.J.** (1986) Thrust tectonic controls on Miocene alluvial fan distribution patterns, southern Pyrenees. In: *Foreland Basins* (Ed. P. Homewood), *IAS Spec. Publ.*, **8,** 247–258.

Hodgetts, D., Egan, S.S. and **Williams, G.D.** (1998) Flexural modelling of continental lithosphere deformation: a comparison of 2D and 3D techniques. *Tectonophysics*, **294,** 1–20.

Houston, W.S., Huntoon, J.E. and **Kamola, D.L.** (2000) Modelling of Cretaceous foreland-basin parasequences, Utah, with implications for timing of Sevier thrusting. *Geology*, **28,** 267–270.

Hovius, N., Stark, C.P. and **Allen, P.A.** (1997) Sediment flux from a mountain belt derived by landslide mapping. *Geology*, **25,** 231–234.

Howard, A.D. (1994) A detachment limited model of drainage basin evolution. *Water Resour. Res.*, **30,** 739–752.

Howard, A.D., Dietrich, W.E. and **Seidl, M.A.** (1994) Modeling fluvial erosion on regional to continental scales. *J. Geophys. Res.*, **99,** 19971–13986.

Humphrey, N.F. and **Heller, P.L.** (1995) Natural oscillations in coupled geomorphic systems: an alternative origin for cyclic sedimentation. *Geology*, **23,** 499–502.

Jin, J., Aigner, T., Bachman, G.H., Luterbacher and **Muller, M.** (1995) Sequence stratigraphy and depositional history in the south-eastern German Molasse Basin. *Mar. Petrol. Geol.*, **12,** 929–940.

Johnson, D.D. and **Beaumont, C.** (1995) Preliminary results from a planform kinematic model of orogen evolution, surface processes and the development of clastic foreland basin stratigraphy. In: *Stratigraphic Evolution of Foreland Basins* (Eds S. Dorobek and G. Ross), *SEPM Spec. Publ.*, **52,** 3–24.

Kenyon, P.M. and **Turcotte, D.L.** (1985) Morphology of delta prograding by bulk sediment transport. *GSA Bull.*, **84,** 1457–1465.

Kirby, E., Reiners, P.W., Krol, M.A., Whipple, K.X., Hodges, K.V., Farley, K.A., Tang, W. and **Chen, Z.** (2002) Late Cenozoic evolution of the eastern margin of the Tibetan Plateau: inferences from 40Ar/39Ar and (U-Th)/He thermochronology. *Tectonics*, **21,** 10.1029/2000TC001246.

Koss, J.E., Ethridge, F.G. and **Schumm, S.A.** (1994) An experimental study of the effects of baselevel change on fluvial, coastal and shelf systems. *J. Sed. Res.*, **B64,** 90–98.

Kuenen, P.H. (1957) Longitudinal filling of oblong sedimentary basins. *Verhandelingen van het Koninklijk Nederlandsch Geologische – Mijnbouwkundig Genootschap. Gedenkboek F.A. Vening Meinesz*, **18,** 189–195.

Leopold, L.B. and **Maddock, T., Jr** (1953) The hydraulic geometry of stream channels and some physiographic implications. *USGS Prof. Paper*, **252,** 57.

Mackey, S.D. and **Bridge, J.S.** (1995) Three-dimensional model of alluvial stratigraphy: theory and application. *J. Sed. Res.*, **B65,** 7–31.

Marr, J.G., Swenson, J.B., Paola, C. and **Voller, V.R.** (2000) A two diffusion model of fluvial stratigraphy in closed depositional basins. *Basin Res.*, **12,** 381–398.

Marzo, M., Nijman, W. and **Puigdefàbregas, C.** (1988) Architecture of the Castissent fluvial sheet sandstones, Eocene South Pyrenees, Spain. *Sedimentology*, **35,** 719–738.

Meigs, A.J. (1997) Sequential development of a selected Pyrenean thrust fault. *J. Struct. Geol.*, **19,** 481–502.

Meigs, A., Brozovoic, N. and **Johnson, M.L.** (1999) Steady, balanced rates of uplift and erosion of the Santa Monica Mountains, California. *Basin Res.*, **11,** 59–73.

Meijer, X.D. (2002) Modelling the drainage evolution of a river-shelf system forced by Quaternary glacio-eustacy. *Basin Res.*, **14,** 361–379.

Miall, A.D. (1981) Alluvial sedimentary basins: tectonic setting and basin architecture. In: *Sedimentation and Tectonics in Alluvial Basins* (Ed. A.D. Miall), *Geol. Assoc. Can. Spec. Paper*, **23,** 1–33.

Milliman, J.D. and **Syvitski, J.P.M.** (1992) Geomorphic/tectonic control of sediment discharge to the oceans: the importance of small mountainous rivers. *J. Geol.*, **100,** 525–544.

Molenaar, N. and **Martinius, A.W.** (1996) Fossiliferous intervals and sequence boundaries in shallow marine fan-deltaic deposits (Early Eocene, southern Pyrenees, Spain). *Palaeogeogr. Palaeoclimatol. Palaeoecol.*, **121,** 147–168.

Morris, R.G. and **Sinclair, H.D.** (1997) Exhumation of the Pyrenean Orogen: implications for sediment discharge. *Basin Res.*, **101,** 69–85.

Murray, A.B. and **Paola, C.** (1997) Properties of a cellular braided-stream model. *Earth Surf. Proc. Land.*, **22,** 1001–1025.

Mutti, E., Seguret, M. and **Sgavetti, M.** (1988) Sedimentation and deformation in the Tertiary sequences of the southern Pyrenees. In: *AAPG Mediterranean Basin Conference, Spec. Publ. Geol. Parma Univ. Field Trip*, **7,** 153pp.

Nijman, W. (1998) Cyclicity and basin axis shift in a piggyback basin: towards modelling of the Eocene Tremp-Ager Basin, South Pyrenees, Spain. In: *Cenozoic Foreland Basins of Western Europe* (Eds A. Mascle, C. Puigdefàbregas, H.P. Luterbacher and M. Fernandez), *Geol. Soc. London Spec. Publ.*, **134,** 135–162.

Nijman, W. and **van Oosterhout, C.W.M.** (1994) *Quantative model study of a thrust sheet-top basin, The Eocene Tremp-Ager Basin.* Stratigraphic Database prepared for Shell Research, Rijswijk, NL. Institute of Earth Sciences, Utrecht University, Utrecht, 99 pp.

Ori, G.G. (1993) Continental depositional systems of the Quaternary of the Po Plain (northern Italy). *Sed. Geol.*, **83,** 1–14.

Oualine, S. (1997) *Practical C Programming*, 3rd edn. O'Reilly, Cambridge, 428 pp.

Paola, C. (2000) Quantitative models of sedimentary basin filling. *Sedimentology* **47** (s1), 121–178 (doi: 10.1046/j.1365-3091.2000.00006.x).

Paola, C., Heller, P.L. and **Angevine, C.L.** (1992) The large-scale dynamics of grain size variations in alluvial basins I. Theory. *Basin Res.*, **4,** 73–90.

Peper, T. and **de Boer, P.L.** (1995) Intrabasinal thrust-tectonic versus climate control on rhythmicities in the Eocene South Pyrenean Tremp-Graus Foreland Basin; inferences from forward modelling. *Tectonophysics*, **249,** 93–107.

Plint, A.G. (1991) High-frequency relative sea-level oscillations in Upper Cretaceous shelf clastics of the Alberta Foreland Basin. In: *Tectonics and Eustasy* (Ed. D.I.M. Macdonald), *Int. Assoc. Sedimentol. Spec. Publ.*, **12,** 409–428.

Plint, A.G., McCarthy, P.J. and **Faccini, U.F.** (2001) Nonmarine sequence stratigraphy; updip expression of sequence boundaries and system tracts in a high-resolution framework, Cenomanian Dunvegan Formation, Alberta foreland basin, Canada. *AAPG Bull.*, **85,** 1967–2001.

Posamentier, H.W. and **Vail, P.R.** (1988) Eustatic controls on clastic deposition I – sequence and system tracts models. In: *Sea-Level Changes: an Integrated Approach* (Eds C.K. Wilgus, B.S. Hastings, C.A. Ross, H.W. Posamentier, J.C. Van Wagoner and G.S.C. Kendall), *SEPM Spec. Publ.*, **42,** 109–124.

Puigdefàbregas, C. and **Souquet, P.** (1986) Tectono-sedimentary cycles and depositional sequences of the Mesozoic and Tertiary from the Pyrenees. *Tectonophysics*, **129,** 173–203.

Quiquerez, A., Allemand, P. and **Dromart, G.** (2000) Dibafill; a 3-D two-lithology diffusive model for basin infilling. *Comp. Geosci.*, **26,** 1029–1042.

Ramos, E., Busquets, P. and **Vergéz, J.** (2002) Interplay between longitudinal fluvial and transverse alluvial fan systems and growing thrusts in a piggyback basin (SE Pyrenees). *Sed. Geol.*, **146,** 105–131.

Remacha, E., Fernandez, L.P., Meastro, E., Oms, O., Estrada, O. and **Teixell, A.** (1998) The upper Hecho Group turbidites and their vertical evolution to deltas. In: *Field Trip Guidebook of the 15th International Sedimentological Congress* (Eds A.M. Hevia and A.R. Soria), Alicante, Spain.

Ritchie, B., Hardy, S. and **Gawthorpe, R.** (1999) Three-dimensional modelling of coarse-grained clastic deposition in sedimentary basins. *J. Geophys. Res.*, **104,** 17759–17780.

Robinson, R.A.J. and **Slingerland, R.L.** (1998) Origin of grain-size trends in a foreland basin: the Ponoco Formation of the Central Appalachian basin. *J. Sed. Res.*, **68,** 473–486.

Schlager, W. (1993) Accommodation and supply – a dual control on stratigraphic sequences. *Sed. Geol.*, **86,** 111–136.

Schlunegger, F., Jordan, T.E. and **Klaper, E.M.** (1997) Controls of erosional denudation in the orogen on foreland basin evolution; the Oligocene central Swiss Molasse basin as an example. *Tectonics*, **16,** 823–840.

Schmidt, K.M. and **Montgomery, D.R.** (1995) Limits to relief. *Science*, **270,** 617–620.

Schumm, S.A. (1963) Disparity between present rates of denudation and orogeny. *USGS Prof. Paper*, **454-H,** H1–H13.

Schwans, P. (1995) Controls on sequence stacking and fluvial to shallow-marine architecture in a foreland basin. *AAPG Bull.*, **64,** 55–102.

Shanley, K.W. and **McCabe, P.J.** (1994) Perspectives on the sequence stratigraphy of continental strata. *AAPG Bull.*, **78,** 544–568.

Sinclair, H.D. and **Allen, P.A.** (1992) Vertical versus horizontal motions in the Alpine orogenic wedge: stratigraphic response in the foreland basin. *Basin Res.*, **4,** 215–232.

Sinclair, H.D., Coackley, D.P., Allen, P.A. and **Watts, A.B.** (1991) Simulation of foreland basin stratigraphy using a diffusion model of mountain belt uplift and erosion: an example of the Central Alps, Switzerland. *Tectonics*, **10,** 599–620.

Sinha, R. and **P.F. Friend** (1994) River systems and their sediment flux, Indo-Gangetic plains, north Bihar, India. *Sedimentology*, **41,** 825–845.

Slingerland, R.L., Harbaugh, J.W. and **Furlong, K.P.** (1993) *Simulating Clastic Sedimentary Basins*. Prentice Hall, New York, 220pp.

Small, E.E., Anderson, R.S., Hancock, G.S. and **Finkel, R.C.** (1999) Estimates of regolith production from 10Be and 26Al: Evidence for steady state alpine hillslopes. *Geomorphology*, **27,** 131–150.

Spangler, M.G. and **Handy, R.L.** (1982) *Soil Engineering*. Harper & Row Publishing, New York, 819 pp.

Stock, J.D. and **Montgomery, D.R.** (1999) Geologic constraints on bedrock river incision using the streampower law. *J. Geophys. Res.*, **104,** 4983–4993.

Syvitski, J.P.M. and **Daughney, S.** (1992) Delta2: Delta progradation and basin filling. *Comp. Geosci.*, **18/7,** 839–879.

Tucker, G.E. (1996) *Modelling the large-scale interaction of climate, tectonics and topography*. PhD Thesis, Pennsylvania State University, University Park, PA.

Tucker, G.E. and **Slingerland, R.** (1996) Predicting sediment flux from fold and thrust belts. *Basin Res.* **8,** 329–350.

Tucker, G.E. and **Whipple, K.X.** (2002) Topographic outcomes predicted by stream erosion models: sensitivity analysis and inter-model comparison. *J. Geophys. Res.*, **107,** 2179. DOI: 10.1029/2001JB000162.

Van Wagoner, J.C., Posamentier, H.W., Mitchum, R.M., Vail, P.R., Sarg, J.F., Loutit, T.S. and **Hardenbol, J.** (1988) An overview of the fundamentals of sequence stratigraphy and key definitions. In: *Sea-Level Changes: an Integrated Approach* (Eds C.K. Wilgus, B.S. Hastings, C.G. Kendall, H.W. Posamentier, C.A. Ross and J.C. Van Wagoner), *SEPM Spec. Publ.*, **42,** 39–45.

Wees, J.D. and **Cloetingh, S.** (1994) A finite-difference technique to incorporate spatial variations in rigidity and planar faults into 3-D models for lithospheric flexure. *Geophys. J. Int.*, **117,** 179–195.

Weltje, G.J., van Ansenwoude, S.O.K.J. and **de Boer, P.L.** (1996) High-frequency detritical signals in Eocene fan-delta sandstones of mixed parentage (South-Central Pyrenees, Spain): are construction of chemical weathering in transit. *J. Sed. Res.*, **66,** 119–131.

Wescott, W.A. (1993) Geomorphic thresholds and complex response of fluvial systems – some implications for sequence stratigraphy. *AAPG Bull.*, **77,** 1208–1218.

Whipple, K.X. and **Tucker, G.E.** (1999) Dynamics of the stream power river incision model: implications for the height limits of mountain ranges, landscape response timescales, and research needs. *J. Geophys. Res.*, **104,** 17661–17674.

Whipple, K.X. and **Tucker, G.E.** (2002) Implications of sediment-flux-dependent river incision models for landscape evolution. *J. Geophys. Res.*, **107,** B2. DOI: 10.1029/2000JB000044.

Willgoose, G.R., Bras, R.L. and **Rodriguez-Iturbe, I.** (1991) A physically coupled network and hillslope evolution model. *Water Resour. Res.*, **27,** 1671–1684.

Zweigel, J., Aigner, T. and **Luterbacher, H.P.** (1998) Eustatic versus tectonic controls on Alpine foreland fill, sequence stratigraphy and subsidence analysis in the SE German Molasse. In: *Cenozoic Foreland Basins in Western Europe* (Eds A. Mascle, C. Puigdefàbregas, H.P. Luterbacher and M. Fernandez), *Geol. Soc. London Spec. Publ.*, **134,** 299–323.

Manuscript received 21 November 2002;
revision accepted 18 March 2004.